arXiv:0905.3511v1 [astro-ph.SR] 21 May 2009

# A Search for Carbon-Chain-Rich Cores in Dark Clouds

Tomoya HIROTA, and Masatoshi OHISHI

*National Astronomical Observatory of Japan, Mitaka, Tokyo 181-8588, JAPAN*

*tomoya.hirota@nao.ac.jp*

Satoshi YAMAMOTO

*Department of Physics, The University of Tokyo, Bunkyo-ku, Tokyo 113-0033, JAPAN*

## ABSTRACT

We present results of a survey of CCS, $HC_3N$, and $HC_5N$ toward 40 dark cloud cores to search for "Carbon-Chain–Producing Regions(CCPRs)", where carbon-chain molecules are extremely abundant relative to $NH_3$, as in L1495B, L1521B, L1521E, and the cyanopolyyne peak of TMC-1. We have mainly observed toward cores where the $NH_3$ lines are weak, not detected, or not observed in previous surveys, and the CCS, $HC_3N$, and $HC_5N$ lines have been detected toward 17, 17, and 5 sources, respectively. Among them, we have found a CCPR, L492, and its possible candidates, L1517D, L530D, L1147, and L1172B. They all show low abundance ratios of $[NH_3]/[CCS]$ (hereafter called the $NH_3$/CCS ratio) indicating the chemical youth. Combining our results with those of previous surveys, we have found a significant variation of the $NH_3$/CCS ratio among dark cloud cores and among molecular cloud complexes. Such a variation is also suggested by the detection rates of carbon-chain molecules. For instance, the $NH_3$/CCS ratios are higher and the detection rates of carbon-chain molecules are lower in the Ophiuchus cores than in the Taurus cores. An origin of these systematic abundance variation is discussed in terms of the difference in the evolutionary stage or the contraction timescale. We have also identified a carbon-chain-rich star-forming core, L483, where intense $HC_3N$ and $HC_5N$ lines are detected. This is a possible candidate for a core with "Warm Carbon-Chain Chemistry".

*Subject headings:* ISM:Abundances — ISM:Molecules: — Molecular Processes

## 1. Introduction

One of the outstanding characteristics of dark cloud cores, which are formation sites of low-mass stars, is high abundances of carbon-chain molecules. Suzuki et al. (1992) carried out survey observations of CCS, $HC_3N$, $HC_5N$, and $NH_3$ toward 49 dense cores, and found that the abundance of CCS is anticorrelated with that of $NH_3$, which is interpreted in terms of chemical evolution of dark cloud cores; CCS and $NH_3$ are abundant in early and late stages of chemical evolution, respectively (Suzuki et al. 1992). Similar survey observations were carried out for dense molecular cloud cores (Fuente et al. 1990; Benson et al. 1998;

Lai & Crutcher 2000), Bok globules and Herbig Ae/Be stars (Scappini & Codella 1996), translucent clouds (Turner et al. 1998), low-mass young stellar objects associated with $H_2O$ masers (de Gregorio-Monsalvo et al. 2006), and infrared dark clouds (Sakai et al. 2008b), as well as individual clouds such as the Pipe Nebula (Rathborne et al. 2008), the Perseus molecular cloud (Rosolowsky et al. 2008), and the Orion molecular cloud (Tatematsu et al. 2008), revealing a relationship between physical and chemical evolutionary stages of molecular cloud cores. A number of detailed studies on the dark cloud cores using the CCS lines were also conducted (e.g., Hirahara et al. 1992; Velusamy et al. 1995; Kuiper et al. 1996; Ohashi et al. 1999; Lai et al. 2003). These results clearly demonstrated that the distribution of CCS is anticorrelated with those of $NH_3$ and $N_2H^+$. In particular, dynamically evolved cores such as L1498 and L1544, which are gravitationally infalling in the central part of the cores, show a donut-like distribution of CCS due to its depletion in gas phase, while the $NH_3$ and $N_2H^+$ distributions are centrally condensed (Kuiper et al. 1996; Ohashi et al. 1999). Such a chemically differentiated feature is successfully interpreted in terms of chemical and dynamical evolution of dark cloud cores through recent detailed theoretical studies (e.g., Bergin & Langer 1997; Aikawa et al. 2001, 2003, 2005).

In the CCS survey by Suzuki et al. (1992), four "Carbon-Chain–Producing Regions" (CCPRs) were identified: L1495B, L1521B, L1521E, and the cyanopolyyne peak of TMC-1. In CCPRs, the CCS and other carbon-chain molecules are extremely abundant while $NH_3$ is deficient, suggesting that they are chemically less evolved (Suzuki et al. 1992). Recent comprehensive observational studies on CCPRs revealed that they are dynamically younger than other starless cores (Hirota et al. 2002, 2004; Tafalla & Santiago 2004). Thus, detailed studies on such sources are of great importance to understand initial conditions of low-mass star formation processes.

However, only four CCPRs have been identified to date, all of which are in the Taurus molecular cloud. This is partly because most of the previous studies on dark cloud cores were based on the survey of the $NH_3$ lines (Benson & Myers 1989) and the samples were primarily chosen from the $NH_3$ cores (e.g., Benson et al. 1998). In order to establish the chemical evolutionary scheme of dark cloud cores on a statistical basis, we need to know how frequently CCPRs show up.

With this in mind, we carried out a survey of the CCS, $HC_3N$, and $HC_5N$ lines toward dark cloud cores where the $NH_3$ lines are weak, not detected, or not observed in the previous surveys, considering that the abundances of carbon-chain molecules are anticorrelated with that of $NH_3$ (Suzuki et al. 1992). As a result, we found a new candidate for a CCPR, L492 in the Aquila rift, whose details were already published (Hirota & Yamamoto 2006). In addition, we have reanalyzed previous observations of the CCS and $NH_3$ lines, part of which were published (e.g., Hirota et al. 2001). All the data are used for the statistical analysis of the chemical evolution of dark cloud cores. Although our study is not based on unbiased survey observations, it would be useful to establish the chemical evolutionary scenario.

## 2. Observations

Observations were conducted with the 45 m radio telescope at Nobeyama Radio Observatory (NRO) in 2002 March and 2004 April. The observed lines are summarized in Table 1. The CCS ($J_N$=$4_3$-$3_2$), $HC_3N$ ($J$=5-4), and $HC_5N$ ($J$=17-16) lines in the 45 GHz region were simultaneously observed with an SIS mixer receiver whose system temperature was 200-300 K. The main-beam efficiency ($\eta_{mb}$) and the half-power beam width were 0.7 and 37″, respectively. In addition, we observed the CCS and $NH_3$ lines in the 22-23 GHz region toward selected sources, L1400B, L1517D, L492, L429-2, L483, L530D, L1147, and L1172B, in order to search for $NH_3$ toward the CCS peak. These lines were observed simultaneously with a HEMT receiver whose system temperature was about 200 K. The main-beam efficiency and the beam size were 0.8 and 74″, respectively. Acousto-optical radio spectrometers with the frequency resolution of 37 kHz were used as the backend. Pointing was checked by observing nearby SiO maser sources every two hours, and the pointing accuracy was estimated to be better than 5″rms. Observations in 2002 March were performed with the position-switching mode with the off position of 10′ in the azimuth direction. On the other hand, the frequency-switching mode was employed for the observations in 2004 April, with the frequency throw of 0.4 MHz for the off-signal spectrum.

Observed sources are summarized in Table 2. We selected these sources mainly from the list of the $NH_3$ survey by Benson & Myers (1989), where the $NH_3$ lines are not detected or not intense in spite of the existence of a dense core traced by the $C^{18}O$ line (Myers et al. 1983). Furthermore, we selected the sources where the $NH_3$ lines were not observed by Benson & Myers (1989), whereas the CS lines were detected (Lee et al. 2001). In total, we observed 32 dark cloud cores, among which five sources contain *IRAS* point sources and the others are starless. They include five sources, L1523, L183(N), L1719B, B68, and L483 where the CCS lines were previously observed (Suzuki et al. 1992; Lai et al. 2003; Benson et al. 1998). Two sources, L1495C and L1172D, were later identified to be previously known sources, L1495N and L1172A, respectively.

For most of the sources, we made five-point mapping observations around the reference positions, (0″, 0″), (+80″, +80″), (+80″, -80″), (-80″, +80″), and (-80″, -80″), in order not to miss the spectral lines, because the peak position of the core might often be shifted from the reference position by more than the beam size of 37″. For cores where at least one of the lines was detected at any position, we further searched for the positions with stronger intensity with a grid spacing of 40″. An example of the profile map obtained is shown in Figure 1. It should be noted that cores smaller than about 80″ in diameter might be missed from detection in our observations due to the coarse-sampling observations.

In addition, we analyzed results of our previous survey of CCS, $HC_3N$, and $HC_5N$ toward eight sources, L1527, L1512, L183(S), L1696A, L1689N, L1157, L1155C, and L1228, as listed in Table 3. For these sources, the results for CCS were reported by Hirota et al. (2001). Observations were made in 1998 and 1999 with the 45 m radio telescope at NRO. Details of the observations were similar to those of the sessions in 2002 and 2004. However, we observed these sources only toward the reference positions, except for L1512 where we carried out mapping observations of CCS and $HC_3N$. We observed the CCS and $HC_3N$ lines

toward all of the eight sources while $HC_5N$ was observed only toward L1527.

In total, we finally obtained 40 samples of dark cloud cores both with and without the *IRAS* point sources.

## 3. Results

Examples of the observed spectra are shown in Figures 2 and 3. We detected both the CCS and $HC_3N$ lines toward 17 out of 40 samples, and detected the $HC_5N$ lines toward five sources out of 35 samples. Among our sources, detection of the $NH_3$ lines was reported for 24 sources out of 39 sources, mainly by Benson & Myers (1989) and the present study. All of these detections indicate that there exist dense cores with the $H_2$ densities of the order of $10^4$ cm$^{-3}$ (Benson & Myers 1989; Suzuki et al. 1992). On the other hand, none of the CCS, $HC_3N$, $HC_5N$, and $NH_3$ lines were detected toward 14 out of our 40 samples probably due to insufficient sensitivity of our observations, and/or positional offset from the intensity peak. Some of these cores might have densities less than the critical densities of the observed lines, $\sim 10^4$ cm$^{-3}$.

A few of them show intense spectra of carbon-chain molecules. In particular, we found remarkably intense spectra of CCS, $HC_3N$, and $HC_5N$ lines toward L492. Brightness temperatures of these lines toward L492 were comparable to those toward the known CCPRs such as L1495B, L1521B, L1521E, and the cyanopolyyne peak of TMC-1 (e.g., Suzuki et al. 1992). This result strongly suggests that L492 would be extremely rich in carbon-chain molecules, which was confirmed by follow-up observations (Hirota & Yamamoto 2006).

### 3.1. Abundances of the Observed Molecules

For all of the detected lines, peak antenna temperature, line width, and LSR velocity are derived by fitting the Gaussian profile to each spectrum, which are summarized in Table 4. For the $NH_3$ lines toward L429-1 and L483, we derived the LSR velocities and the line widths assuming that they are common for all the hyperfine components. Because of the insufficient spectral resolution of 37 kHz, which is larger than most of the hyperfine splittings due to the H nuclei in the $NH_3$ (1,1) line, we fitted only the five major spectral components as labeled in Table 1 (Ungerechts et al. 1980). The line widths and LSR velocities are slightly different from molecule to molecule for some sources. This is partly due to the hyperfine structure of the $HC_3N$ and $NH_3$ lines, whose line widths tend to be broader than those of the other molecules.

Using these line parameters, column densities of CCS, $HC_3N$, $HC_5N$, and $NH_3$ were calculated by the similar method described by Suzuki et al. (1992). In addition, we calculated column densities of $NH_3$ for cores that we did not observe, using the results of Benson & Myers (1989) if they are available. The dipole moments of CCS, $HC_3N$, $HC_5N$, and $NH_3$ were assumed to be 2.81, 3.72, 4.33, and 1.46 Debye, respectively (Murakami 1990; Lafferty & Lovas 1978; Alexander et al. 1976; Cohen & Poynter 1974). The LTE condition

was assumed, and the excitation temperatures were fixed to 5 K for CCS and 6.5 K for $HC_3N$, $HC_5N$, and $NH_3$. In this paper, we do not use the results of $J_N$=$2_1$-$1_0$ lines of CCS, because the beam size at the 22 GHz band, 74″, is almost comparable to the typical size of the observed dark cloud cores as shown in Figure 4, and the derived column densities may be affected due to the unknown source coupling efficiency.

The derived column densities are summarized in Table 5. For L492, line parameters and column densities are taken from Hirota & Yamamoto (2006). Calculated optical depths,$\tau$, of the observed lines were 0.17-3.4, 0.07-8.8, and 0.15-0.65 for the CCS, $HC_3N$, and $HC_5N$ lines, respectively. The CCS and $HC_5N$ lines were found to be optically thin ($\tau < 1$), except for the CCS line toward L492 ($\tau = 3.4$; Hirota & Yamamoto 2006). On the other hand, the $HC_3N$ lines are optically thick toward L1527 ($\tau = 2.4$), L1512 ($\tau = 1.5$), B68 ($\tau = 1.0$), L492 ($\tau = 8.8$; Hirota & Yamamoto 2006), and L483 ($\tau = 1.5$). For L492, the optical depth and excitation temperatures were derived from the intensity ratio of the hyperfine components of the $HC_3N$ line (Hirota & Yamamoto 2006).

In order to estimate uncertainties in the derived column densities, we calculated the column densities of CCS, $HC_3N$, and $HC_5N$ by varying the assumed excitation temperature of $\pm 1$ K. We found that the uncertainties in the derived column densities were typically 10%-30%. In addition, we compared column densities of some of the sources where the CCS lines were observed previously. We found that the column densities of CCS toward these sources differ by a factor of 0.4-3 mostly due to the difference in the observed positions, as in the case of L1512 and B68, for instance. Considering these results, we estimate that the uncertainties in the derived molecular column densities are typically about 30%-40%, while it could be as high as a factor of 3 in the worst case.

### 3.2. Distributions of the Observed Molecules

For several sources where the CCS and $HC_3N$ lines are intense, we obtained integrated intensity maps as shown in Figure 4. Detailed descriptions for individual sources are summarized in Appendix A. The CCS and $HC_3N$ maps show similar morphology (Hirahara et al. 1992; Tafalla et al. 2006), although some of them show slight differences in their sizes and peak positions. It is well known that CCS and some carbon-chain molecules are depleted at the central part of a starless dense core, and their distributions show a central hole (Velusamy et al. 1995; Kuiper et al. 1996; Ohashi et al. 1999; Lai & Crutcher 2000; Lai et al. 2003). We can see such an apparent hole only in the CCS map of L1172D, possibly due to the lack of significant depletion of CCS and $HC_3N$ in other mapped sources. However, it is also likely that we could not trace such a small structure in the cores because of the large beam size and the coarse grid spacing of our mapping observations, 40″, which are comparable to or slightly larger than the expected size of the hole. In fact, the central hole of CCS in B335 was not detected by the single dish observation, but was first imaged by the interferometric observation using the VLA (Velusamy et al. 1995) with the spatial resolution of 12″. Further high-resolution observations would settle this issue.

## 4. Discussions

### 4.1. Possible Candidates for CCPRs

In the present survey, we observed the CCS, $HC_3N$, and $HC_5N$ lines toward 40 dark cloud cores, and found several dense cores with high column densities of carbon-chain molecules and/or extremely low $NH_3$/CCS ratios. Here we tentatively define the CCPR as the core with the $NH_3$/CCS ratio of less than 10, which can easily be distinguished from other cores in Table 5 and Figure 5 as discussed later. Based on this criterion, we can identify five new candidates for CCPRs, L492, L1517D, L530D, L1147, and the northeast clump of L1172B, as well as four known CCPRs, L1495B, L1521B, L1521E, and the cyanopolyyne peak of TMC-1 (Suzuki et al. 1992). As briefly described in the Appendix A, the chemical compositions of the newly found sources show a mutual variation, and are different from originally identified CCPRs. Here we classify the newly found candidates into two groups and summarize their properties below.

One of the most outstanding source is L492, where the carbon-chain molecules have high column densities comparable to the known CCPRs. The high abundances of carbon-chain molecules, the lack of significant depletion, and low deuterium fractionation all suggest chemically less evolved nature of L492 (Hirota & Yamamoto 2006, and Appendix A.8). Contrary to the other CCPRs, the $NH_3$ lines are also detected in L492 with moderate intensities. Furthermore, L492 is thought to be dynamically evolved according to a strong infalling signature found in the spectral lines (Lee et al. 2001). Detailed discussions in Hirota & Yamamoto (2006) concluded that L492 is chemically and dynamically evolved than other CCPRs, while younger than prestellar cores such as L1498 and L1544 (Kuiper et al. 1996; Ohashi et al. 1999). This order does not always mean the absolute age, because timescales of contraction, gas phase chemistry, and depletion would be different from source to source.

The other group of the sources with remarkably low $NH_3$/CCS ratios are the starless cores L1517D, L530D, and L1147, as well as the northeast clump of L1172B. In these sources, the $NH_3$/CCS ratios are comparable to those of other known CCPRs, although column densities of both of CCS and $NH_3$ are generally lower than the known CCPRs as can be seen in Table 5. Therefore, they are possible candidates for CCPRs. In the case of L1147, the weak $NH_3$ line is detected toward the dust continuum peak, and the CCS peak coincides with the same position (see Appendix A.12), which results in the low $NH_3$/CCS ratio toward the central part of the dense core as in the case of L492. However, the column densities of both CCS and $NH_3$ in L1147 are one order of magnitude lower than those of L492. Because the dust continuum emission of L1147 is weaker than the other cores (Kirk et al. 2005), it is also likely that the column density of $H_2$ is also less than L492. On the other hand, in L1517D and L530D, the peak positions of CCS are located at the edge of dense cores, which would be a reason for the lower column densities of the observed molecules (see Appendices A.4 and A.11). Therefore, it cannot be ruled out the possibility that the CCS line in L1517D and L530D would trace the outer part of the dense core, as can be seen in L1498 and L1544 (Kuiper et al. 1996; Ohashi et al. 1999). For L1172B, dust continuum maps are not available in our knowledge, and hence, we will not discuss further the relationships between the CCS, $HC_3N$, $NH_3$, and dust continuum emission (see Appendix A.14).

In summary, L492 has been confirmed as a definitive CCPR that is found for the first time outside the Taurus molecular cloud, and the others are possible candidates for CCPRs, for which further high resolution mapping observations of carbon-chain molecules and $NH_3$, together with the dust continuum emission, are necessary for confirmation.

### 4.2. Detection Rate of the Carbon-Chain Molecules and $NH_3$

According to our results, overall detection rates of the observed molecular lines are 43% (17/40), 43% (17/40), 14%(5/35), and 62%(24/39) for CCS, $HC_3N$, $HC_5N$, and $NH_3$, respectively, which are slightly lower than those of Suzuki et al. (1992), 55%, 67%, 31%, and 80%, respectively, as listed in Table 6. Although we selectively observed the cores with low abundance of $NH_3$, based on the anticorrelation between carbon-chain molecules and $NH_3$ (Suzuki et al. 1992), the detection rates of carbon-chain molecules are not so high as expected. Most of the observed cores with weak $NH_3$ emission, except for five newly found candidates as mentioned in the previous section, are turned out to have "normal" $NH_3$/CCS ratios and hence, would be just low column density objects. As mentioned previously, none of the observed lines were detected toward some of our samples probably due to offsets from the real emission peak. Otherwise, they would have less densities so that the $NH_3$ lines along with those of carbon-chain molecules are hardly excited. These results mean that the CCPRs are intrinsically rare even in the Taurus region where four CCPRs have already been identified .

As discussed in the previous section, we calculated the column densities of CCS, $HC_3N$, $HC_5N$, and $NH_3$ by the similar method described by Suzuki et al. (1992). This enables us to discuss statistically about the carbon-chain chemistry in dark cloud cores by combining our results with those of previous surveys (Suzuki et al. 1992; Benson & Myers 1989; Benson et al. 1998; Hirota et al. 2001) supplemented with several individual observations (e.g., Hirota et al. 2002, 2004), which were made by almost the same method of observations and data analysis. Details of our samples are discussed in the Appendix B. We compiled a sample of nearby dark cloud cores consisting of 90 sources in total for the further statistical studies. The total detection rates are 53%, 55%, 23%, and 74% for CCS, $HC_3N$, $HC_5N$, and $NH_3$, respectively.

As noted in the Introduction, the CCPRs have so far been detected only in the Taurus molecular cloud (Suzuki et al. 1992). This result would suggest a difference in the overall chemical compositions from cloud to cloud. Hence, it is worthy to compare the detection rates of carbon-chain molecules between the Taurus and other regions in order to investigate whether such a chemical abundance variation occurs. Because the numbers of available samples are sufficient only for the Taurus and Ophiuchus cores ($\sim$30 each), we here summarize the results for these two regions in Table 6. It is easily found that the detection rates of carbon-chain molecules are significantly lower in the Ophiuchus cores than in the Taurus cores. A ratio of the number of the CCS cores relative to that of the $NH_3$ cores in the Taurus region is three times higher than that of the Ophiuchus region, as listed in Table 6. Since our sample was not prepared in an unbiased way, these results are not statistical in a strict

sense. Nevertheless, we can extract 'statistical' trends from the results because the sample involves a number of sources with and without star-forming activities. Therefore, it is very likely that carbon-chain molecules are generally less abundant in the Ophiuchus cores than in the Taurus cores.

We also compared our results with those of recent complete survey of CCS and $NH_3$ in the Pipe Nebula (Rathborne et al. 2008) and the Perseus molecular cloud (Rosolowsky et al. 2008), as listed in Table 6. Detection rates of the observed molecules are different from region to region. In the Pipe Nebula, the detection rate of CCS is lower than that in the Taurus region and is comparable to that in the Ophiuchus region, while the detection rate of $NH_3$ is almost the same as those in the other regions. On the other hand, the detection rate of CCS in the Perseus region is rather close to that in the Taurus region, and the detection rate of $NH_3$ in the Perseus region is the highest among our four sampled regions. Although the methods of the surveys are different from ours in various ways, such as observed transitions, sensitivities, spectral and spatial resolutions, methods of data analysis, and definition of star formation activities (association of *IRAS* and/or *Spitzer* sources), the possible difference in the ratio of the number of the CCS cores relative to that of the $NH_3$ cores can be seen in Table 6; the ratio in the Taurus region (90%) is nearly 3, 2, and 1.5 times higher than that in the Ophiuchus region, the Pipe Nebula, and the Perseus region, respectively, which would be indicative of difference in an average chemical age of cores in each region, as discussed later (Suzuki et al. 1992).

### 4.3. Variation in the $NH_3$/CCS Ratio

In order to investigate a source-to-source variation in molecular abundances, we focus on the abundance ratio of $NH_3$/CCS, which is recognized as a useful probe of the chemical evolutionary stage of dark cloud cores (Suzuki et al. 1992). Following the discussion by Ohishi & Kaifu (1998), we investigate the relationship between the CCS abundance and the $NH_3$/CCS ratio in Figure 5. We plotted the sources where either the CCS or $NH_3$ line is detected (Table A.1). Because of the lack of a complete data set for the column densities of $H_2$ for all the cores, we plot the column densities of CCS instead of the fractional abundance of CCS relative to $H_2$. Therefore, a scatter in the column density of CCS is not only due to the variation in the fractional abundance of CCS relative to $H_2$, but is also attributed to the difference in the column density of $H_2$.

In Figure 5, we can find CCPRs (L1495B, L1521B, L1521E, the cyanopolyyne peak of TMC-1, and L492) at the upper-left part, and the CCPR candidates (L1517D, L530D, L1147, and the (-40″, -40″) and (+40″, +40″) positions in L1172B) at the middle-left part. We stress that there is no carbon-chain-rich cores in the Ophiuchus region as depicted in Figure 5(d), even though we have almost the same number of samples as in the Taurus region. Such a systematic abundance variation from cloud to cloud has been found in the deuterium fractionation ratios of $DNC/HN^{13}C$ (Hirota et al. 2001) and $N_2D^+/N_2H^+$ (Crapsi et al. 2005).

We again refer to the results of the Pipe Nebula (Rathborne et al. 2008) and the Perseus molecular cloud (Rosolowsky et al. 2008). It can be found that there is no carbon-chain-

rich core in the Perseus region in spite of the completeness of their survey, as shown in Figure 6. On the other hand, we find several candidates for CCPRs in the Pipe nebula (Rathborne et al. 2008), where the $NH_3$/CCS ratios are less than 10. In the Pipe nebula, there exists a dense core (core 37 of Rathborne et al. 2008) where the CCS line is detected while $NH_3$ is not. Because of the lack of the $NH_3$ data, it is not plotted in Figure 6(b). The column density of CCS toward this core is derived to be $2.0\times10^{12}$ cm$^{-2}$ (Rathborne et al. 2008). Although this value is much lower than those of the known CCPRs, it would be a possible candidate of a CCPR. This result would suggest that the cores in the Pipe nebula are generally in the early stages of both chemical and dynamical evolution (Rathborne et al. 2008).

Although the above discussions are not based on unbiased, complete, and uniform surveys, the apparent region-to-region variation of the chemical composition would be indicative of difference in chemical and/or physical properties of each region. In fact, chemical and dynamical model calculations demonstrate that molecular abundances and distributions could reflect the physical properties and their initial conditions of the cores such as the density, degree of depletion, and velocity structure of the cores (Aikawa et al. 2001, 2003, 2005). Observational evidences for the variations of physical properties are reported by Jijina et al. (1999) based on the database of a survey of the $NH_3$ lines. Such a variation of the core properties would affect not only chemistry but also star-formation processes, which results in either isolated or clustered mode, and low-mass or high-mass star-formation.

### 4.4. Possible Origin of Chemical Abundance Variation

In the above sections, we recognize significant source-to-source chemical abundance variation, in particular between the Taurus and Ophiuchus regions. Here we discuss two possible scenarios which can explain qualitatively the systematic difference in the molecular abundances between the Taurus cores and Ophiuchus ones.

#### *4.4.1. Difference in Ages of the Cores*

Most simply, the difference in the chemical abundances between the Taurus and Ophiuchus regions can be interpreted in terms of the different age of the Taurus molecular cloud complex itself from that of Ophiuchus. Due to its younger chemical evolutionary stage of the Taurus region than in Ophiuchus, more young cores which have been just formed in the cloud complex could still remain in the Taurus region than in Ophiuchus.

One would think that if CCPRs are the precursors of the normal dense cores, the fraction of CCPRs over normal cores would represent the duration or the age of the CCPR phase. Such a statistical estimation is valid only for the Taurus region because the number of both sample cores, CCPRs and normal ones, are available only in this region. If we simply assume a typical lifetime of starless $NH_3$ and/or CCS cores where the typical $H_2$ density is an order of $10^4$ cm$^{-3}$ (Suzuki et al. 1992), to be (2-10)$\times10^5$ yr (e.g., Figure 2 in Ward-Thompson et al. 2007), the CCPR phase would last no longer than $\sim$(0.4-2)$\times10^5$ yr.

The lifetime is determined from the fraction of CCPRs with respect to all the starless cores, 4/20, in our sample. This value is in good agreement with the ratio of the duration of CCPRs and other cores, $\sim 4 \times 10^5$ yr and $\sim 20 \times 10^5$ yr, respectively, estimated from a chemical model calculations and previous observational results (Ohishi & Kaifu 1998). Thus, our statistically estimated lifetime of the CCPR phase in the Taurus cores is consistent with that of theoretical prediction.

If stars as well as cores have been forming steadily at a constant rate in both the Taurus and Ophiuchus regions with the same evolutionary timescale, we would expect to detect three CCPRs (∼20%) among 15 starless cores in our Ophiuchus sample (Table 6). None detection of CCPRs in the Ophiuchus region would imply that there is no core younger than $\sim 10^5$ yr in Ophiuchus, although we cannot completely rule out the possibility of a selection bias. In other words, dense core formation in Ophiuchus might have stopped since $\sim 10^5$ yr ago which results in a true deficient of CCPRs in the Ophiuchus region. A similar picture is proposed by Jørgensen et al. (2008) on the basis of the fact that fraction of embedded young stellar objects is relatively lower in the Ophiuchus region than in Perseus. However, there still remains sufficient amount of molecular gas traced by the $^{13}$CO and C$^{18}$O lines (Tachihara et al. 2000) which have potential to form more dense cores, and hence, it seems unlikely that the dense core formation has stopped over $\sim 10^5$ yr.

### *4.4.2. Difference in Contraction Timescales of the Cores*

Another possible scenario for the systematic molecular abundance variations is that the difference in the contraction timescale between the Taurus cores and Ophiuchus cores. The contraction timescale would reflect the physical properties such as average density, magnetic field strength and/or turbulence in/around the cores (e.g., Aikawa et al. 2001, 2003, 2005). According to the detailed theoretical model calculations, behaviors of molecular abundances and their distributions are predicted to depend strongly on the timescale of the gravitational contraction; the longer contraction time would result in the less abundances of carbon-chain molecules at the central part of the core (Aikawa et al. 2001, 2003, 2005). Therefore, the systematically lower abundances of carbon-chain molecules in the Ophiuchus cores could be accounted for by the slower contraction than in the Taurus cores.

Previous works have shown that the star-formation activity in the Ophiuchus region seems to be remarkably different from that in Taurus. There exist an active cluster-forming region in Ophiuchus triggered by a nearby Scorpius OB association, while only isolated star-formation can be seen in Taurus (e.g., Ward-Thompson et al. 2007). As a consequence, one would expect slower contraction timescale in the Taurus region than in Ophiuchus, which is exactly the opposite of what we are proposing in this section. However, active cluster-formation is localized only around "the main body" in the $\rho$-Ophiuchus molecular cloud or a dark cloud L1688, and rest of the region shows rather inactive star-formation (Tachihara et al. 2000). In fact, overall star-formation efficiency in the Ophiuchus region, in particular Ophiuchus north region, is lower than in Taurus (Tachihara et al. 2000). Based on the survey of the C$^{18}$O line in the Ophiuchus region, timescale of starless cores in the

Ophiuchus region is estimated to be $8\times10^5$ yr, which is four times longer than that in Taurus, $2\times10^5$ yr (Tachihara et al. 2000). It is consistent with our hypothesis that the contraction timescale in Taurus is generally shorter than in Ophiuchus. This difference might be related to the difference in the line widths of the $C^{18}O$ lines which reflect turbulence of the cores; mean line widths are 0.49, 0.9, and 0.7 km $s^{-1}$ for the Taurus, $\rho$-Ophiuchus main body, and Ophiuchus north regions, respectively (Tachihara et al. 2000).

One might suppose that the difference in initial conditions can be an origin of chemical abundance variation. Due to higher initial densities in the $\rho$-Ophiuchus main body than in Taurus (Jijina et al. 1999; Tachihara et al. 2000), chemical evolution in the molecular cloud could occur prior to dense core formation in the $\rho$-Ophiuchus main body. In this case, cores in the $\rho$-Ophiuchus main body would be formed from already processed gas (e.g., higher $NH_3$/CCS ratios), while Taurus ones from more pristine material (lower $NH_3$/CCS ratio). This could produce the observed dichotomy without any need for a faster core contraction in Taurus. Higher initial density in the $\rho$-Ophiuchus main body region would results in faster gravitational contraction than in Taurus, giving a high star-formation rate. However, it is predicted that initial density of molecular cloud prior to the core formation ($< 10^4$ $cm^{-3}$) would not much affect the molecular abundances in the dense core (Aikawa et al. 2003). Therefore, we prefer the possible scenario of the faster contraction in the Taurus regions than in Ophiuchus rather than the difference in the initial densities.

In our samples, there are five cores which are embedded in the $\rho$-Ophiuchus main body, L1681A, L1681B, L1690, L1696A, and L1696B (Table A.1). Among them, only L1681B and L1696A were detected in the $NH_3$ line with normal $NH_3$/CCS ratios while other cores were not detected probably due to the position offset from real core center. Further complete survey of the Ophiuchus cores (e.g., L1689B observed by Lee et al. 2003) is still an important issue to shed light on chemical and dynamical timescale of dense cores in this region.

The difference in timescale of evolution of dense cores and young stellar objects is also proposed by Jørgensen et al. (2008) based on the comparison of young stellar objects and dense cores in the Ophiuchus and Perseus regions. Thus, it is interesting to compare statistically physics and chemistry of dense cores and young stellar objects between Taurus and Ophiuchus regions.

The difference in the contraction timescale is also reflected in the molecular distributions of CCS and $NH_3$ in the observed cores. In general, depletion of molecules at the central part of the core is more significant for the slower contraction case, and hence, the size of the central hole of the distribution of CCS becomes larger (Aikawa et al. 2001, 2003, 2005). In contrast, cores with fast contraction show centrally condensed distribution of CCS without significant depletion (Aikawa et al. 2005). For instance, a chemical and dynamical model with a faster contraction is preferable for L1521E, one of the CCPRs, (Aikawa et al. 2005) judging from its central density, chemical composition along with no signature of depletion, and slightly broader line width than in other prestellar cores. In our mapping observations, CCS distributions in two carbon-chain rich cores in the Aquila region, L492 and L483, are found to be centrally peaked structure. The contraction timescales of the L492 and L483 cores would have been short although they are dynamically evolved; L492 is in the dynam-

ically collapsing (Lee et al. 2001; Hirota & Yamamoto 2006) and L483 has already formed Class 0 protostar (Fuller et al. 1995). They may be even shorter than those of the Taurus cores considering the possible difference in the chemical and dynamical evolutionary stages of the cores between the Aquila rift and the Taurus region, as suggested by Hirota & Yamamoto (2006).

In order to clarify the difference in the evolutionary timescale and/or age between the Aquila region and the Taurus region, it is crucial to observe the distribution of CCS in L492 and L483, as well as the known CCPRs in the Taurus molecular cloud, with the higher resolution interferometers. Such observations would enable us to confirm whether there are really no central holes of CCS in these cores (e.g., Velusamy et al. 1995). Although it is difficult to infer the timescale or the age of each core quantitatively, our results would provide some hints to understand the timescale of the formation and evolution of dark cloud cores.

### 4.5. Warm Carbon-Chain Chemistry

Finally, we comment on Warm Carbon-Chain Chemistry (WCCC) recently proposed by Sakai et al. (2008a). The WCCC is first identified in L1527 and is characterized by high abundances of long carbon-chain molecules such as $C_nH$ ($n$=4,5,6) and $C_nH_2$ ($n$=3,4,6), and intense spectra of higher excitation lines of carbon-chain molecules. According to these criteria, L483 is considered to be a possible candidate of the WCCC source. When it is compared with L1527, the both are associated with the *IRAS* point source, and the $NH_3$/CCS ratios are relatively high due to high $NH_3$ column density. The abundances of $HC_3N$ are remarkably high and are comparable to those of CCPRs such as L1495B, L1521B, L1521E, the cyanopolyyne peak of TMC-1, and L492. Furthermore, we stress that L483 and L1527 show stronger emission of longer carbon-chain molecule $HC_5N$ than those in CCPRs. Except for relatively high abundance of CCS, chemistry in L483 seems to be quite similar to that in L1527. Observational studies of WCCC have just been started, and hence, the reason for such similarities and differences will be investigated in the near future (Sakai et al. 2008a, 2009). Interestingly, the regions where the WCCC sources are found, Taurus (L1527) and Aquila (L483), include CCPRs such as L1495B, L1521B, L1521E, the cyanopolyyne peak of TMC-1, and L492. On the other hand, no WCCC sources are found currently in the Ophiuchus and Perseus regions (Sakai et al. 2008a, 2009). Although the discussion is based on a limited number of samples at this moment, the WCCC might have a close connection to the CCPRs. Therefore, chemistry of carbon-chain molecules would be indicative of difference in the physical and chemical properties among molecular cloud complexes.

## 5. Summary

In the present study, we carried out survey observations of CCS, $HC_3N$, and $HC_5N$ toward 40 dark cloud cores in total using the 45 m radio telescope of the NRO. Based on the previous result that the spectra of carbon-chain molecules tend to be intense toward the

cores where the $NH_3$ lines are weak (Suzuki et al. 1992), we primarily observed the dense cores where the $NH_3$ lines are weak, not detected, or not observed previously. The main results of this paper are summarized as follows:

1. We detected the CCS, $HC_3N$, and $HC_5N$ lines for the 17, 17, and 5 cores out of the 40, 40, and 35 cores observed, respectively. According to the previous survey of $NH_3$ conducted by Benson & Myers (1989), the $NH_3$ lines are detected toward 24 cores out of our 40 cores. The detection rates of the CCS, $HC_3N$, and $HC_5N$ lines are lower than those of previous survey (Suzuki et al. 1992), although the spectra of carbon-chain molecules had been expected to be intense toward the cores with weak or no $NH_3$ lines.

2. Among the 40 cores of our survey, we found remarkably intense spectra of CCS, $HC_3N$, and $HC_5N$ toward a starless dense core L492 in the Aquila rift. We have carried out follow-up observations of L492 and found that this source is chemically less evolved dark cloud core like CCPRs.

3. In addition, we found possible candidates for CCPRs, where the $NH_3$/CCS ratios are as low as other known CCPRs: L1517D, L530D, L1147, and L1172B. Further confirmation observations are needed for these sources.

4. Together with the present results, we compiled available results of the survey of carbon-chain molecules and $NH_3$ to investigate the variation of the molecular abundances in the observed samples. We found that the abundance ratios of carbon-chain molecules and $NH_3$, in particular the $NH_3$/CCS ratio, which is a good indicator of chemical evolutionary stage of dark cloud cores, tend to be higher in the Ophiuchus cores than in the Taurus region.

5. The systematic variation can be seen in the detection rates of carbon-chain molecules. For instance, the detection rates of the CCS, $HC_3N$, and $HC_5N$ lines are significantly higher in the Taurus region than in the Ophiuchus region, although the total number of samples, fraction of cores associated with *IRAS* sources, and the detection rate of the $NH_3$ lines are similar to each other.

6. These chemical abundance variation found in our study may suggest the region-to-region difference in the contraction timescale rather than the difference in the evolutionary stage alone, which could be indicative of some differences in the physical properties such as average density, magnetic field strength and/or turbulence in/around the cores.

It is important but difficult to compare evolutionary timescale by the statistical discussion because the present study is not based on the unbiased survey. Further complete and unbiased survey (e.g., Rathborne et al. 2008; Rosolowsky et al. 2008), would be needed to understand low-mass star-formation processes in dark cloud cores both from the chemical and dynamical point of views. Mapping observations of some tracers of chemical evolution

such as carbon-chain molecules, $NH_3$, and deuterated molecules, and submillimeter continuum emission including polarization would also be important to reveal their dynamical and chemical evolutionary stage as proposed in several literatures (e.g., Lee et al. 2003; Shirley et al. 2005; Aikawa et al. 2005; Hirota & Yamamoto 2006).

We are grateful to Miho Ikeda and all the staff of NRO for their assistance in observations. We are also grateful to Nami Sakai for useful discussions about WCCC. We thank the referee for useful suggestions. TH thanks to the Inoue Foundation for Science for the financial support (Research Aid of Inoue Foundation for Science). MO is supported by the Japan Society for the Promotion of Science (JSPS) Core-to-Core program. This study is partly supported by Grant-in-Aid from The Ministry of Education, Culture, Sports, Science and Technology of Japan (No. 14204013, 15071201, and 19024070). The 45 m radio telescope is operated by NRO, a branch of National Astronomical Observatory of Japan.

*Facilities:* No:45m.

## REFERENCES

Aikawa, Y., Herbst, E., Roberts, H., & Caselli, P. 2005, ApJ, 620, 330

Aikawa, Y., Ohashi, N., & Herbst, E. 2003, ApJ, 593, 906

Aikawa, Y., Ohashi, N., Inutsuka, S., Herbst, E., & Takakuwa, S. 2001, ApJ, 552, 639

Alexander, A. J., Kroto, H. W., & Walton, D. R. M. 1976, J. Mol. Spectrosc., 62, 175

Anglada, G., Sepulveda, I., & Gomez, J. F. 1997, A&AS, 121, 255

Bachiller, R., Martin-Píntado, J., & Fuente, A. 1993, ApJ, 417, L45

Bacmann, A., André, P., Puget, J.-L., Abergel, A., Bontemps, S., & Ward-Thompson, D. 2000, A&A, 361, 555

Benson, P. J., Caselli, P., & Myers, P. C. 1998, ApJ, 506, 743

Benson, P. J., & Myers, P. C. 1983, ApJ, 270, 589

Benson, P. J., & Myers, P. C. 1989, ApJS, 71, 89

Bergin, E. A. & Langer, W. D. 1997, ApJ, 486, 316

Brooke, T. Y. et al. 2007, ApJ, 655, 364

Cohen, E. A., & Poynter, R. L. 1974, J. Mol. Spectrosc., 53, 131

Crapsi, A., Caselli, P., Walmsley, C. M., Myers, P. C., Tafalla, M., Lee, C. W., & Bourke, T. L. 2005, ApJ, 619, 379

de Gregorio-Monsalvo, I., Gómez, J. F., Suárez, O., Kuiper, T. B. H., Rodríguez, L. F., & Jiménez-Bailón, E. 2006, ApJ, 642, 319

Enoch, M. L. et al. 2006, ApJ, 638, 293

Fuente, A., Cernicharo, J., Barcia, A., & Gomez-González, J. 1990, A&A, 231, 151

Fuller, G. A. Lada, E. A., Masson, C. R., & Myers, P. C. 1995, ApJ, 453, 754

Hilton, J. & Lahulla, J. F. 1995, A&AS, 113, 325

Hirahara, Y. et al. 1992, ApJ, 394, 539

Hirota, T., Ikeda, M., & Yamamoto, S. 2001, ApJ, 547, 814

Hirota, T., Ito, T., & Yamamoto, S. 2002, ApJ, 565, 359

Hirota, T., Maezawa, H., & Yamamoto, S. 2004, ApJ, 617, 399

Hirota, T., & Yamamoto, S. 2006, ApJ, 646, 258

Hirota, T. et al. 2008, PASJ, 60, 37

Jijina, J., Myers, P. C., & Adams, F. C. 1999, ApJS, 125, 161

Jørgensen, J. K., Johnstone, D., Kirk, H., Myers, P. C., Allen, L. E., & Shirley, Y. L. 2008, ApJ, 683, 822

Kirk, J. M., Ward-Thompson, D., & André, P. 2005, MNRAS, 360, 1506

Kirk, J. M., Ward-Thompson, D., & André, P. 2007, MNRAS, 375, 843

Kuiper, T. B. H., Langer, W. D., & Velusamy, T. 1996, ApJ, 468, 761

Ladd, E. F., Myers, P. C., & Goodman, A. A. 1994, ApJ, 433, 117

Lafferty, W. J. & Lovas, F. J. 1978, J. Phys. Chem. Ref. Data, 7, 441

Lai, S.-P. & Crutcher, R. M. 2000, ApJS, 128, 271

Lai, S.-P., Velusamy, T., Langer, W. D., & Kuiper, T. B. H. 2003, AJ, 126, 311

Lee, C. W., & Myers, P. C. 1999, ApJS, 123, 233

Lee, C. W., Myers, P. C., & Tafalla, M. 2001, ApJS, 136, 703

Lee, J. -E., Evans, N. J. II., Shirley, Y. L., & Tatematsu, K. 2003, ApJ, 583, 789

Loinard, L., Torres, R. M., Mioduszewski, A. J., & Rodríguez, L. F. 2008, ApJ, 675, L29

Mundy, L. G., Wootten, H. A. Wilking, B. A. 1990, ApJ, 352, 159

Murakami, A. 1990, ApJ, 357, 288

Myers, P. C., Heyer, M., Snell, R. L., & Goldsmith, P. F. 1988, ApJ, 324, 907

Myers, P. C., Linke, R. A., & Benson, P. J. 1983, ApJ, 264, 517

Ohashi, N., Lee, S. W., Wilner, D. J., & Hayashi, M. 1999, ApJL, 518, L41

Ohishi, M., & Kaifu, N. 1998, in Chemistry and Physics of Molecules and Grains in Space ( London: Royal Society of Chemistry), 205

Rathborne, J. M., Lada, C. J., Muenchi, A. A., Alves, J. F., & Lombardi, M. 2008, ApJS, 174, 396

Rosolowsky, E. W., Pineda, J. E., Foster, J. B., Borkin, M. A., Kauffmann, J., Caselli, P., Myers, P. C., & Goodman, A. A. 2008, ApJS, 175, 509

Sakai, N., Sakai, T., Hirota, T., Burton, M. G., & Yamamoto, S. 2009, ApJ, 697, 769

Sakai, N., Sakai, T., Hirota, T., & Yamamoto, S. 2008a, ApJ, 672, 371

Sakai, T., Sakai, N., Kamegai, K., Hirota, T., Yamaguchi, N., Shiba, S., & Yamamoto, S. 2008b, ApJ, 678, 1049

Scappini, F. & Codella, C. 1996, MNRAS, 282, 587

Shirley, Y. L., Nordhaus, M. K., Grcevich, J. M., Evans, N. J. II., Rawlings, J. M. C., & Tatematsu, K. 2005, ApJ, 632, 982

Suzuki, H., Yamamoto, S., Ohishi, M., Kaifu, N., Ishikawa, S., Hirahara, Y., & Takano, S. 1992, ApJ, 392, 551

Tachihara, K., Mizuno, A., & Fukui, Y. 2000, ApJ, 528, 817

Tafalla, M., & Santiago, J. 2004, A&A, 414, L53

Tafalla, M. Santiago-García, J., Myers, P. C., Caselli, P., Walmsley, C. M., & Crapsi, A. 2006, A&A, 455, 577

Tatematsu, K., Kandori, R., Umemoto, T., & Sekimoto, Y. 2008, PASJ, 60, 407

Torres, R. M., Loinard, L., Mioduszewski, A. J., & Rodríguez, L. F. 2007, ApJ, 671, 1813

Turner, B. E., Lee, H. -H., & Herbst, E. 1998, ApJS, 115, 91

Ungerechts, H., Walmsley, C. M., & Winnewisser, G. 1980, A&A, 88, 259

Velusamy, T., Kuiper, T. B. H., & Langer, W. D. 1995, ApJ, 451, L75

Ward-Thompson, D., André, P., Crutcher, R., Johnstone, D., Onishi, T., & Wilson, C. 2007, in Protostars and Planets V, eds. B. Reipurth, D. Jewitt, & K. Keil (Tucson: University of Arizona Press), 33

Yamamoto, S., Shuji, S., Kawaguchi, S., Chikada, Y., Suzuki H., Kaifu, N., Ishikawa, S., & Ohishi, M. 1990, ApJ, 361, 318

This preprint was prepared with the AAS LaTeX macros v5.2.

Table 1. Observed Lines

| Molecule | Transition | $\nu$ (MHz) | $S_{ul}$[b] | $\mu$ (Debye) | Reference |
|---|---|---|---|---|---|
| CCS | $J_N$=$2_1$-$1_0$ | 22344.033 | 1.98 | 2.81 | 1,2 |
| | $J_N$=$4_3$-$3_2$ | 45379.033 | 3.97 | 2.81 | 1,2 |
| $HC_3N$ | $J$=5-4 | 45490.316[a] | 5.00 | 3.72 | 3 |
| $HC_5N$ | $J$=17-16 | 45264.721 | 17.00 | 4.33 | 4 |
| $NH_3$ | (1,1;VH)[c] | 23692.955 | ··· | ··· | ··· |
| | (1,1;H)[c] | 23693.895 | ··· | ··· | ··· |
| | (1,1;M)[c] | 23694.496 | 1.50 | 1.46 | 5 |
| | (1,1;L)[c] | 23695.095 | ··· | ··· | ··· |
| | (1,1;VL)[c] | 23696.037 | ··· | ··· | ··· |

[a]Main hyperfine component

[b]Intrinsic line strength

[c]Hyperfine components are blended. Each component is labeled as adopted by Ungerechts et al. (1980).

References. — 1: Murakami (1990); 2: Yamamoto et al. (1990); 3: Lafferty & Lovas (1978); 4: Alexander et al. (1976); 5: Cohen & Poynter (1974)

Table 2. Observed Sources

| Source Name | $\alpha$(J2000) ( h m s) | $\delta$(J2000) ( ° ′ ″) | *IRAS* Number | Reference | Date |
|---|---|---|---|---|---|
| L1495C | 04 13 30.7 | +28 15 55 | 04108+2803 | 1 | 2002 Mar. |
| L1495D | 04 14 18.2 | +28 15 52 | ··· | 1 | 2002 Mar. |
| L1506 | 04 18 31.1 | +25 19 25 | ··· | 1 | 2002 Mar. |
| L1400B | 04 24 46.6 | +55 01 52 | ··· | 1 | 2002 Mar. |
| L1400E | 04 28 28.5 | +54 47 36 | ··· | 1 | 2002 Mar. |
| L1400F | 04 29 51.4 | +54 14 19 | ··· | 1 | 2002 Mar. |
| L1551A | 04 30 58.1 | +18 17 10 | ··· | 1 | 2002 Mar. |
| L1551 | 04 31 30.0 | +18 12 30 | 04287+1806 | 1 | 2002 Mar. |
| L1445 | 04 32 07.0 | +46 37 23 | ··· | 2 | 2002 Mar. |
| L1517D | 04 55 48.1 | +30 38 46 | ··· | 1 | 2004 Apr. |
| L1523 | 05 06 22.9 | +31 41 19 | ··· | 1 | 2002 Mar. |
| L1778A | 15 39 27.5 | −07 10 08 | ··· | 1 | 2002 Mar. |
| L183(N) | 15 54 09.2 | −02 49 42 | ··· | 3 | 2002 Mar. |
| L1721 | 16 14 28.2 | −18 54 44 | ··· | 1 | 2002 Mar. |
| L1719B | 16 22 12.4 | −19 38 41 | ··· | 1 | 2002 Mar. |
| L1690 | 16 27 46.4 | −24 16 59 | ··· | 1 | 2002 Mar. |
| L1709A | 16 30 50.8 | −23 41 03 | ··· | 1 | 2002 Mar. |
| L1709C | 16 33 53.4 | −23 38 32 | ··· | 1 | 2002 Mar. |
| L158 | 16 47 23.2 | −13 59 21 | 16445-1352 | 1 | 2002 Mar. |
| L191 | 16 47 29.3 | −12 28 38 | ··· | 1 | 2002 Mar. |
| L204F | 16 47 48.4 | −11 56 56 | ··· | 1 | 2002 Mar. |
| B68 | 17 22 38.8 | −23 50 02 | ··· | 1 | 2002 Mar. |
| L492 | 18 15 46.1 | −03 46 13 | ··· | 2 | 2002 Mar.[a] |
| L429-1 | 18 17 05.6 | −08 13 30 | ··· | 2 | 2004 Apr. |
| L483 | 18 17 29.7 | −04 39 38 | 18148-0440 | 4 | 2004 Apr. |
| L530H | 18 49 28.5 | −04 57 40 | ··· | 1 | 2002 Mar. |
| L530D | 18 49 57.3 | −04 49 49 | ··· | 1 | 2004 Apr. |
| L1147 | 20 40 31.8 | +67 21 45 | ··· | 1 | 2004 Apr. |
| L1155H | 20 43 06.5 | +67 46 26 | ··· | 1 | 2002 Mar. |
| L1155D | 20 43 49.8 | +67 36 29 | ··· | 1 | 2002 Mar. |
| L1172D | 21 02 09.0 | +67 53 54 | 21017+6742 | 1 | 2002 Mar. |
| L1172B | 21 03 32.0 | +68 11 58 | ··· | 1 | 2002 Mar. |

[a]Follow-up observations were carried out in 2003 February and 2004 March (Hirota & Yamamoto 2006).

References. — 1: Benson & Myers (1989); 2: Lee et al. (2001); 3: Ungerechts et al. (1980); 4: Benson et al. (1998)

Table 3. Previously Observed Sources

| Source Name[a] | $\alpha$(J2000) ( h m s) | $\delta$(J2000) ( ° ′ ″) | *IRAS* Number | Date |
|---|---|---|---|---|
| L1527 | 04 39 53.6 | +26 03 05 | 04368+2557 | 1998 Apr. |
| L1512 | 05 04 09.7 | +32 43 09 | ··· | 1999 May. |
| L183(S) | 15 54 09.2 | −02 51 39 | ··· | 1999 Feb. |
| L1696A | 16 28 31.5 | −24 19 08 | ··· | 1999 Feb. |
| L1689N | 16 32 22.8 | −24 28 33 | 16293-2422 | 1999 Feb. |
| L1157 | 20 39 06.6 | +68 02 13 | 20386+6751 | 1999 Apr. |
| L1155C | 20 43 30.0 | +67 52 42 | ··· | 1999 Apr. |
| L1228 | 20 59 30.6 | +78 22 49 | 21004+7811 | 1999 Apr. |

[a]All the sources are listed in Hirota et al. (2001).

Table 4. Gauss Fit Parameters for the Detected Sources

| Source Name | ($\Delta\alpha$ ″, $\Delta\delta$ ″) | Line | $T_a^*$ (K) | $v_{lsr}$ (km s$^{-1}$) | $\Delta v$ (km s$^{-1}$) | $T_{rms}$ (K) |
|---|---|---|---|---|---|---|
| L1495C | (+200,-160) | CCS($J_N$=4$_3$-3$_2$) | 0.91(23) | 6.37(8) | 0.60(18) | 0.11 |
| | | $HC_3N$($J$=5-4) | 1.32(14) | 6.38(4) | 0.82(10) | 0.10 |
| | | $HC_5N$($J$=17-16) | <0.33 | ··· | ··· | 0.11 |
| L1400B | (-80,+40) | CCS($J_N$=4$_3$-3$_2$) | 0.61(20) | 3.29(6) | 0.31(12) | 0.07 |
| | | CCS($J_N$=2$_1$-1$_0$) | 0.21(11) | 3.43(14) | 0.52(32) | 0.04 |
| | | $HC_3N$($J$=5-4) | 0.74(13) | 3.33(6) | 0.63(13) | 0.07 |
| | | $HC_5N$($J$=17-16) | <0.20 | ··· | ··· | 0.07 |
| | | $NH_3$(1,1;M) | 0.26(13) | 3.41(28) | 1.09(65) | 0.05 |
| L1527 | (0,0) | CCS($J_N$=4$_3$-3$_2$)[a] | 0.43(17) | 5.85(10) | 0.49(23) | 0.08 |
| | | $HC_3N$($J$=5-4) | 2.34(15) | 6.01(3) | 0.84(7) | 0.08 |
| | | $HC_5N$($J$=17-16) | 0.58(14) | 5.90(7) | 0.57(17) | 0.09 |
| L1517D | (+80,+80) | CCS($J_N$=4$_3$-3$_2$) | 0.42(11) | 5.90(5) | 0.37(12) | 0.05 |
| | | CCS($J_N$=2$_1$-1$_0$) | <0.16 | ··· | ··· | 0.05 |
| | | $HC_3N$($J$=5-4) | <0.14 | ··· | ··· | 0.05 |
| | | $HC_5N$($J$=17-16) | <0.14 | ··· | ··· | 0.05 |
| | | $NH_3$(1,1;M) | <0.13 | ··· | ··· | 0.04 |
| L1512 | (-40,0) | CCS($J_N$=4$_3$-3$_2$) | 0.88(14) | 7.17(3) | 0.33(6) | 0.08 |
| | | $HC_3N$($J$=5-4) | 2.01(61) | 7.15(11) | 0.69(27) | 0.07 |
| | | $HC_5N$($J$=17-16)[b] | ··· | ··· | ··· | ··· |
| L183(N) | (0,0) | CCS($J_N$=4$_3$-3$_2$) | 0.58(43) | 2.49(10) | 0.23(22) | 0.11 |
| | | $HC_3N$($J$=5-4) | 1.42(20) | 2.45(5) | 0.73(12) | 0.10 |
| | | $HC_5N$($J$=17-16) | <0.27 | ··· | ··· | 0.09 |
| L183(S) | (0,0) | CCS($J_N$=4$_3$-3$_2$)[a] | 0.40(19) | 2.53(18) | 0.73(42) | 0.11 |
| | | $HC_3N$($J$=5-4) | 0.63(20) | 2.41(10) | 0.62(23) | 0.11 |
| | | $HC_5N$($J$=17-16)[b] | ··· | ··· | ··· | ··· |
| L1689N | (0,0) | CCS($J_N$=4$_3$-3$_2$)[a] | 0.42(16) | 3.96(11) | 0.57(27) | 0.08 |
| | | $HC_3N$($J$=5-4) | 0.67(11) | 4.02(9) | 1.05(23) | 0.08 |
| | | $HC_5N$($J$=17-16)[b] | ··· | ··· | ··· | ··· |
| B68 | (0,0) | CCS($J_N$=4$_3$-3$_2$) | 0.41(24) | 3.32(9) | 0.30(21) | 0.09 |
| | | $HC_3N$($J$=5-4) | 1.65(17) | 3.37(4) | 0.79(10) | 0.08 |
| | | $HC_5N$($J$=17-16) | 0.38(19) | 3.34(10) | 0.38(23) | 0.09 |
| L492 | (40,0) | CCS($J_N$=4$_3$-3$_2$)[c] | 1.51(10) | 7.73(2) | 0.48(4) | 0.07 |
| | | CCS($J_N$=2$_1$-1$_0$)[c] | 0.69(6) | 7.78(3) | 0.80(8) | 0.03 |
| | | $HC_3N$($J$=5-4)[c] | 2.35(16) | 7.76(3) | 0.81(7) | 0.09 |
| | | $HC_5N$($J$=17-16)[c] | 1.23(12) | 7.76(2) | 0.49(6) | 0.06 |
| | (0,0) | $NH_3$(1,1;VH)[c,d] | 0.19(7) | 7.87(4) | 0.86(10) | 0.04 |
| | | $NH_3$(1,1;H)[c,d] | 0.31(7) | 7.87(4) | 0.86(10) | 0.04 |
| | | $NH_3$(1,1;M)[c,d] | 0.74(8) | 7.87(4) | 0.86(10) | 0.04 |
| | | $NH_3$(1,1;L)[c,d] | 0.33(7) | 7.87(4) | 0.86(10) | 0.04 |
| | | $NH_3$(1,1;VL)[c,d] | 0.24(7) | 7.87(4) | 0.86(10) | 0.04 |
| L429-1 | (0,-40) | CCS($J_N$=4$_3$-3$_2$) | 0.76(10) | 6.85(5) | 0.66(11) | 0.11 |
| | | $HC_3N$($J$=5-4) | 0.78(16) | 6.77(9) | 0.88(21) | 0.08 |
| | | $HC_5N$($J$=17-16) | <0.24 | ··· | ··· | 0.08 |
| | (0,0) | $NH_3$(1,1;VH)[d] | 0.47(12) | 6.87(7) | 1.43(17) | 0.09 |
| | | $NH_3$(1,1;H)[d] | 0.59(12) | 6.87(7) | 1.43(17) | 0.09 |
| | | $NH_3$(1,1;M)[d] | 1.05(13) | 6.87(7) | 1.43(17) | 0.09 |
| | | $NH_3$(1,1;L)[d] | 0.46(12) | 6.87(7) | 1.43(17) | 0.09 |
| | | $NH_3$(1,1;VL)[d] | 0.35(12) | 6.87(7) | 1.43(17) | 0.09 |
| L483 | (0,0) | CCS($J_N$=4$_3$-3$_2$) | 0.84(25) | 5.31(8) | 0.49(17) | 0.15 |
| | | CCS($J_N$=2$_1$-1$_0$) | 0.36(16) | 5.36(22) | 1.00(56) | 0.06 |
| | | $HC_3N$($J$=5-4) | 2.03(18) | 5.35(4) | 0.85(9) | 0.12 |
| | | $HC_5N$($J$=17-16) | 0.75(21) | 5.23(6) | 0.40(14) | 0.12 |
| | | $NH_3$(1,1;VH)[d] | 1.16(13) | 5.54(3) | 1.06(6) | 0.05 |
| | | $NH_3$(1,1;H)[d] | 1.18(13) | 5.54(3) | 1.06(6) | 0.05 |

Table 4—Continued

| Source Name | ($\Delta\alpha$ ″, $\Delta\delta$ ″) | Line | $T_a^*$ (K) | $v_{lsr}$ (km s$^{-1}$) | $\Delta v$ (km s$^{-1}$) | $T_{rms}$ (K) |
|---|---|---|---|---|---|---|
| | | $NH_3$(1,1;M)[d] | 2.16(14) | 5.54(3) | 1.06(6) | 0.05 |
| | | $NH_3$(1,1;L)[d] | 1.35(13) | 5.54(3) | 1.06(6) | 0.05 |
| | | $NH_3$(1,1;VL)[d] | 0.86(13) | 5.54(3) | 1.06(6) | 0.05 |
| L530D | (+80,+40) | CCS($J_N$=$4_3$-$3_2$) | 0.36(15) | 3.26(10) | 0.47(24) | 0.08 |
| | | CCS($J_N$=$2_1$-$1_0$) | <0.11 | ··· | ··· | 0.04 |
| | | $HC_3N$($J$=5-4) | <0.20 | ··· | ··· | 0.07 |
| | | $HC_5N$($J$=17-16) | <0.20 | ··· | ··· | 0.07 |
| | | $NH_3$(1,1;M) | <0.08 | ··· | ··· | 0.03 |
| L1157 | (0,0) | CCS($J_N$=$4_3$-$3_2$)[a] | <0.13 | ··· | ··· | 0.04 |
| | | $HC_3N$($J$=5-4) | 0.18(3) | 2.71(9) | 0.96(6) | 0.04 |
| | | $HC_5N$($J$=17-16)[b] | ··· | ··· | ··· | ··· |
| L1147 | (0,-80) | CCS($J_N$=$4_3$-$3_2$) | 0.54(18) | 2.79(7) | 0.40(17) | 0.08 |
| | | CCS($J_N$=$2_1$-$1_0$) | 0.25(08) | 2.81(10) | 0.56(22) | 0.03 |
| | | $HC_3N$($J$=5-4) | 0.64(12) | 2.80(6) | 0.66(14) | 0.06 |
| | | $HC_5N$($J$=17-16) | <0.22 | ··· | ··· | 0.07 |
| | | $NH_3$(1,1;M) | 0.08(8) | 2.64(26) | 0.46(56) | 0.02 |
| L1155C | (0,0) | CCS($J_N$=$4_3$-$3_2$)[a] | 0.34(13) | 2.80(12) | 0.64(29) | 0.05 |
| | | $HC_3N$($J$=5-4) | 0.30(9) | 2.84(12) | 0.81(28) | 0.05 |
| | | $HC_5N$($J$=17-16)[a] | ··· | ··· | ··· | ··· |
| L1228 | (0,0) | CCS($J_N$=$4_3$-$3_2$)[a] | <0.18 | ··· | ··· | 0.06 |
| | | $HC_3N$($J$=5-4) | 0.44(16) | -7.43(10) | 0.53(24) | 0.07 |
| | | $HC_5N$($J$=17-16)[a] | ··· | ··· | ··· | ··· |
| L1172D | (+80,+40) | CCS($J_N$=$4_3$-$3_2$) | 0.20(9) | 2.84(26) | 1.10(61) | 0.07 |
| | | $HC_3N$($J$=5-4) | 1.55(10) | 2.83(3) | 0.98(7) | 0.06 |
| | | $HC_5N$($J$=17-16) | 0.36(12) | 2.84(12) | 0.73(28) | 0.06 |
| L1172B | (-120,-40) | CCS($J_N$=$4_3$-$3_2$) | 0.25(11) | 2.42(17) | 0.71(39) | 0.07 |
| | | CCS($J_N$=$2_1$-$1_0$) | 0.21(08) | 2.26(18) | 0.90(42) | 0.04 |
| | | $HC_3N$($J$=5-4) | 0.51(12) | 2.38(9) | 0.83(22) | 0.06 |
| | | $HC_5N$($J$=17-16) | <0.20 | ··· | ··· | 0.07 |
| | | $NH_3$(1,1;M) | 0.20(5) | 2.48(26) | 1.92(61) | 0.04 |
| | (-40,-40) | CCS($J_N$=$4_3$-$3_2$) | 0.38(16) | 2.36(11) | 0.50(26) | 0.07 |
| | | CCS($J_N$=$2_1$-$1_0$) | 0.17(8) | 2.34(21) | 0.88(48) | 0.03 |
| | | $HC_3N$($J$=5-4) | 0.77(11) | 2.35(06) | 0.76(13) | 0.06 |
| | | $HC_5N$($J$=17-16) | <0.19 | ··· | ··· | 0.06 |
| | | $NH_3$(1,1;M) | <0.12 | ··· | ··· | 0.04 |
| | (+40,+40) | CCS($J_N$=$4_3$-$3_2$) | 0.45(13) | 2.69(9) | 0.58(20) | 0.06 |
| | | CCS($J_N$=$2_1$-$1_0$) | 0.19(10) | 2.75(14) | 0.49(31) | 0.04 |
| | | $HC_3N$($J$=5-4) | 0.45(9) | 2.69(9) | 0.92(22) | 0.06 |
| | | $HC_5N$($J$=17-16) | <0.18 | ··· | ··· | 0.06 |
| | | $NH_3$(1,1;M) | <0.12 | ··· | ··· | 0.04 |

Note. — The numbers in parenthesis represent three times the standard deviation in the Gaussian fit.

[a]Hirota et al. (2001)

[b]Not observed.

[c]Hirota & Yamamoto (2006)

[d]The LSR velocity $v_{lsr}$ and line width $\Delta v$ are common for all the hyperfine components.

Table 5. Column Densities of CCS, $HC_3N$, and $HC_5N$ Determined by the LTE Model

| Source Name | ($\Delta\alpha$ ″, $\Delta\delta$ ″) | $N$[CCS] ($10^{12}$ cm$^{-2}$) | $N$[$HC_3N$] ($10^{12}$ cm$^{-2}$) | $N$[$HC_5N$] ($10^{12}$ cm$^{-2}$) | $N$[$NH_3$] ($10^{14}$ cm$^{-2}$) | $NH_3$/CCS | Reference |
|---|---|---|---|---|---|---|---|
| L1495C | (+200,-160) | 17.2 | 13.8 | <9.0 | 4.0 | 23 | 1,1,1,2 |
| L1495D | (0,0) | <2.2 | <1.4 | <4.9 | <1.0 | ··· | 1,1,1,2 |
| L1506 | (0,0) | <2.8 | <1.7 | <6.2 | <0.5 | ··· | 1,1,1,2 |
| L1400B | (-80,+40) | 5.1 | 5.0 | <5.3 | 0.62 | 12 | 1,1,1,1 |
| L1400E | (0,0) | <2.6 | <1.6 | <5.6 | <0.82 | ··· | 1,1,1,2 |
| L1400F | (0,0) | <2.4 | <1.6 | <5.1 | 0.84 | >35 | 1,1,1,2 |
| L1551A | (0,0) | <2.6 | <1.5 | <5.5 | <0.98 | ··· | 1,1,1,2 |
| L1551 | (0,0) | <2.3 | <1.4 | <5.0 | <0.72 | ··· | 1,1,1,2 |
| L1445 | (0,0) | <2.3 | <1.6 | <5.3 | ··· | ··· | 1,1,1,* |
| L1527 | (0,0) | 5.1 | 47 | 18.9 | 5.0 | 98 | 3,1,1,2 |
| L1517D | (+80,+80) | 3.7 | <1.1 | <3.7 | <0.13 | **<3.5** | 1,1,1,1 |
| L1512 | (-40,0) | 9.0 | 25 | <2.1 | 7.0 | 78 | 1,1,4,4 |
| L1523 | (0,0) | <2.2 | <1.4 | <4.8 | <1.06 | ··· | 1,1,1,2 |
| L1778A | (0,0) | <3.0 | <1.6 | <6.3 | <1.03 | ··· | 1,1,1,2 |
| L183(N) | (0,0) | 3.6 | 13.7 | <7.3 | 16 | 444 | 1,1,1,5 |
| L183(S) | (0,0) | 7.2 | 4.1 | ··· | 32 | 444 | 3,1,*,5 |
| L1721 | (0,0) | <3.1 | <1.8 | <7.0 | <0.81 | ··· | 1,1,1,2 |
| L1719B | (0,0) | <3.3 | <1.8 | <7.0 | <0.87 | ··· | 1,1,1,2 |
| L1690 | (0,0) | <3.1 | <1.8 | <7.0 | <0.72 | ··· | 1,1,1,2 |
| L1696A | (0,0) | <2.7 | <2.1 | <2.0 | 5.0 | >185 | 3,1,6,2 |
| L1709A | (0,0) | <3.3 | <1.8 | <7.2 | 0.99 | >30 | 1,1,1,2 |
| L1689N | (0,0) | 5.8 | 7.5 | ··· | 20 | 345 | 3,1,*,7 |
| L1709C | (0,0) | <3.3 | <1.7 | <6.9 | 1.14 | >35 | 1,1,1,2 |
| L158 | (0,0) | <2.8 | <1.7 | <7.0 | 4.0 | >143 | 1,1,1,2 |
| L191 | (0,0) | <2.8 | <1.7 | <6.4 | 0.71 | >25 | 1,1,1,2 |
| L204F | (0,0) | <2.9 | <1.7 | <6.1 | 1.43 | >49 | 1,1,1,2 |
| B68 | (0,0) | 3.0 | 18.9 | 7.8 | 2.5 | 83 | 1,1,1,2 |
| L492 | (40,0)[a] | 53 | 172 | 41 | 3.4 | **6.4** | 8,8,8,8 |
| L429-1 | (0,-40)[a] | 14.2 | 7.5 | <6.4 | 10.4 | 73 | 1,1,1,1 |
| L483 | (0,0) | 12.3 | 31 | 17.6 | 14.9 | 121 | 1,1,1,1 |
| L530H | (0,0) | <3.8 | <2.0 | <8.4 | <0.65 | ··· | 1,1,1,2 |
| L530D | (+80,+40) | 4.1 | <1.5 | <5.4 | <0.09 | **<2.2** | 1,1,1,1 |
| L1157 | (0,0) | <2.3 | 1.64 | ··· | 5.2 | >226 | 3,1,*,9 |
| L1147 | (0,-80) | 5.5 | 4.5 | <5.9 | 0.08 | **1.5** | 1,1,1,1, |
| L1155H | (0,0) | <2.4 | <1.6 | <5.4 | <0.82 | ··· | 1,1,1,2 |
| L1155C | (0,0) | 5.2 | 2.4 | ··· | 5.0 | 96 | 3,1,*,2 |
| L1155D | (0,0) | <2.8 | <1.6 | <5.7 | <0.34 | ··· | 1,1,1,2 |
| L1228 | (0,0) | <2.4 | 2.3 | ··· | 1.74 | >73 | 3,1,*,2 |
| L1172D | (+80,+40) | 4.9 | 21 | 14.4 | 7.9 | 161 | 1,1,1,2 |
| L1172B | (-120,-40) | 4.0 | 4.4 | <5.2 | 0.81 | 20 | 1,1,1,1 |
| | (-40,-40) | 4.6 | 6.4 | <5.0 | <0.13 | **<2.8** | 1,1,1,1 |
| | (+40,+40) | 6.4 | 4.2 | <4.8 | <0.13 | **<2.0** | 1,1,1,1 |

Note. — Bold letters indicate the $NH_3$/CCS ratios lower than 10, which is a criterion for CCPRs.

[a]Position for the column density of $NH_3$ is (0,0).

References. — 1: Present study; 2: Benson & Myers (1989); 3: Hirota et al. (2001); 4: Suzuki et al. (1992); 5: Ungerechts et al. (1980); 6: Benson & Myers (1983); 7: Mundy et al. (1990); 8: Hirota & Yamamoto (2006); 9: Bachiller et al. (1993)

Table 6. Detection Rate for CCS, $HC_3N$, $HC_5N$, and $NH_3$

| Sample | Total | Star-forming cores | CCS | | $HC_3N$ | | $HC_5N$ | | $NH_3$ | | $\frac{\text{Num. of CCS cores}}{\text{Num. of } NH_3 \text{ cores}}$ |
|---|---|---|---|---|---|---|---|---|---|---|---|
| | | | Detect/Observed | Ratio | Detect/Observed | Ratio | Detect/Observed | Ratio | Detect/Observed | Ratio | |
| Suzuki et al. (1992)[a] | 49 | 22 | 27/49 | 0.55 | 33/49 | 0.67 | 14/49 | 0.29 | 39/49 | 0.80 | 0.69 |
| Present study | 40 | 9 | 17/40 | 0.43 | 17/40 | 0.43 | 5/35 | 0.14 | 24/39 | 0.62 | 0.71 |
| Compiled ensemble | 90 | 34 | 48/90 | 0.53 | 46/83 | 0.55 | 18/80 | 0.23 | 66/89 | 0.74 | 0.73 |
| Taurus | 29 | 9 | 18/29 | 0.62 | 19/29 | 0.66 | 12/29 | 0.41 | 20/29 | 0.69 | 0.90 |
| Ophiuchus | 24 | 9 | 6/24 | 0.25 | 5/21 | 0.24 | 0/22 | 0.00 | 18/24 | 0.75 | 0.33 |
| other than Taurus | 61 | 25 | 30/61 | 0.49 | 27/54 | 0.50 | 6/51 | 0.12 | 37/60 | 0.62 | 0.81 |
| Pipe Nebula[b] | 46 | 1 | 13/46 | 0.28 | ··· | ··· | 4/46 | 0.09 | 29/46 | 0.63 | 0.45 |
| Perseus[c] | 193 | >44 | 96/193 | 0.51 | ··· | ··· | ··· | ··· | 162/193 | 0.84 | 0.59 |

[a]Two sources in the Orion region, L1641N and NGC2071N are included, which are not listed in Table A.1.

[b]Rathborne et al. (2008). We identified the Pipe core 12 as the only the site of star-formation (Brooke et al. 2007).

[c]Rosolowsky et al. (2008). We identified the star-forming cores according to Enoch et al. (2006), which are labeled as "Bolocam" sources in Rosolowsky et al. (2008). We tentatively regard the sources other than "Bolocam" in Rosolowsky et al. (2008) as the starless cores. Therefore, the number of star-forming cores in the Perseus gives a lower limit.

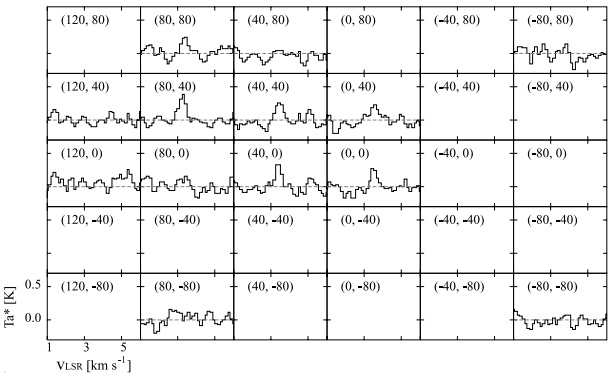


Fig. 1.— Example of the profile map of the CCS lines in L530D.

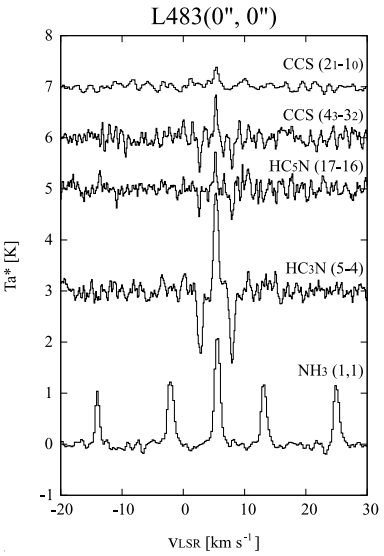


Fig. 2.— Sample spectra of the observed lines in L483. The apparent features below the baseline of the CCS($J_N$=$4_3$-$3_2$), $HC_3N$($J$=5-4), and $HC_5N$($J$=17-16) spectra are artifacts of the frequency-switching technique. All of the five hyperfine components of the $NH_3$(1, 1) line are shown.

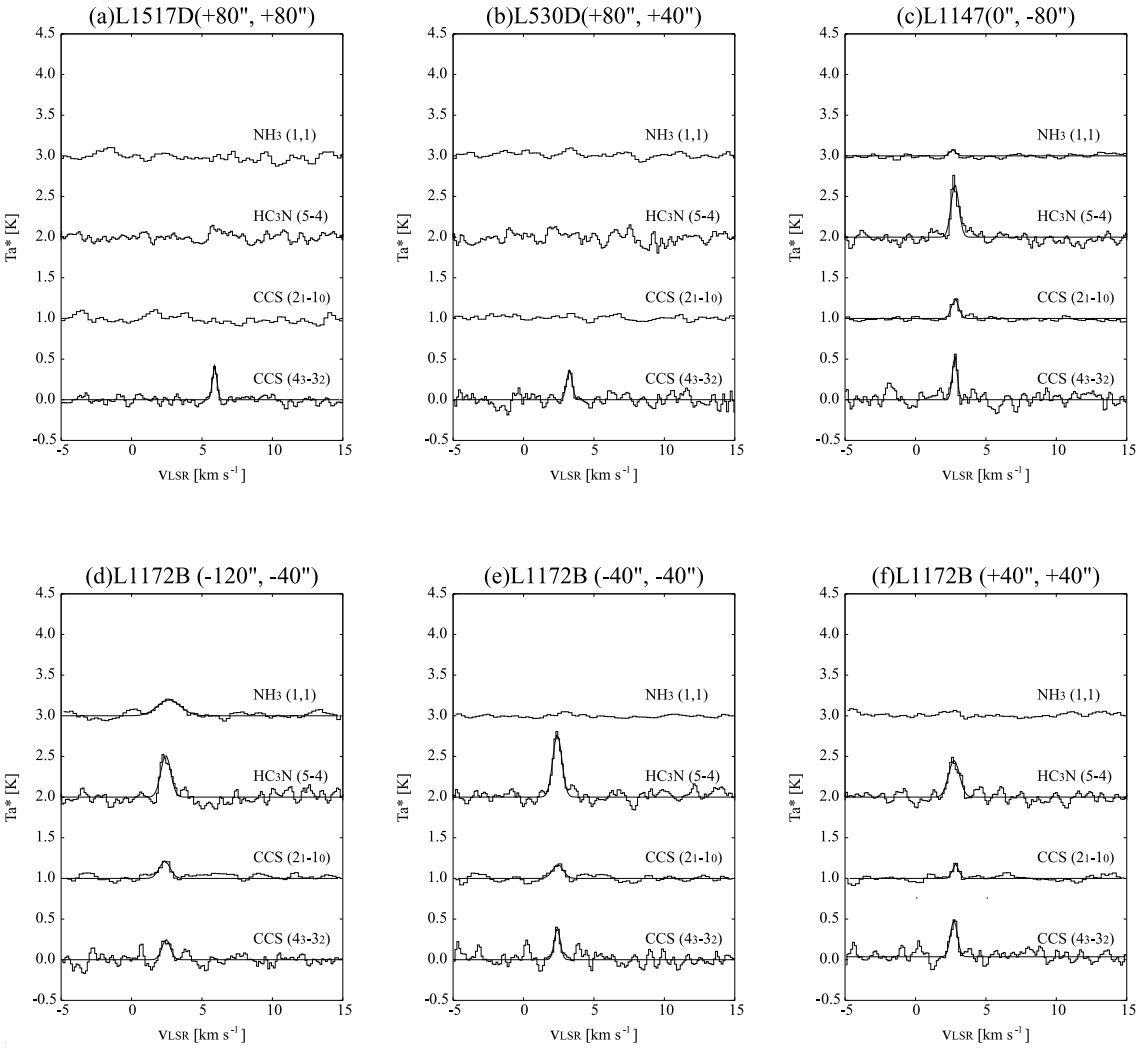


Fig. 3.— Sample spectra of the observed lines in L1517D, L530D, L1147, and L1172B. Results of Gaussian fitting are also shown.

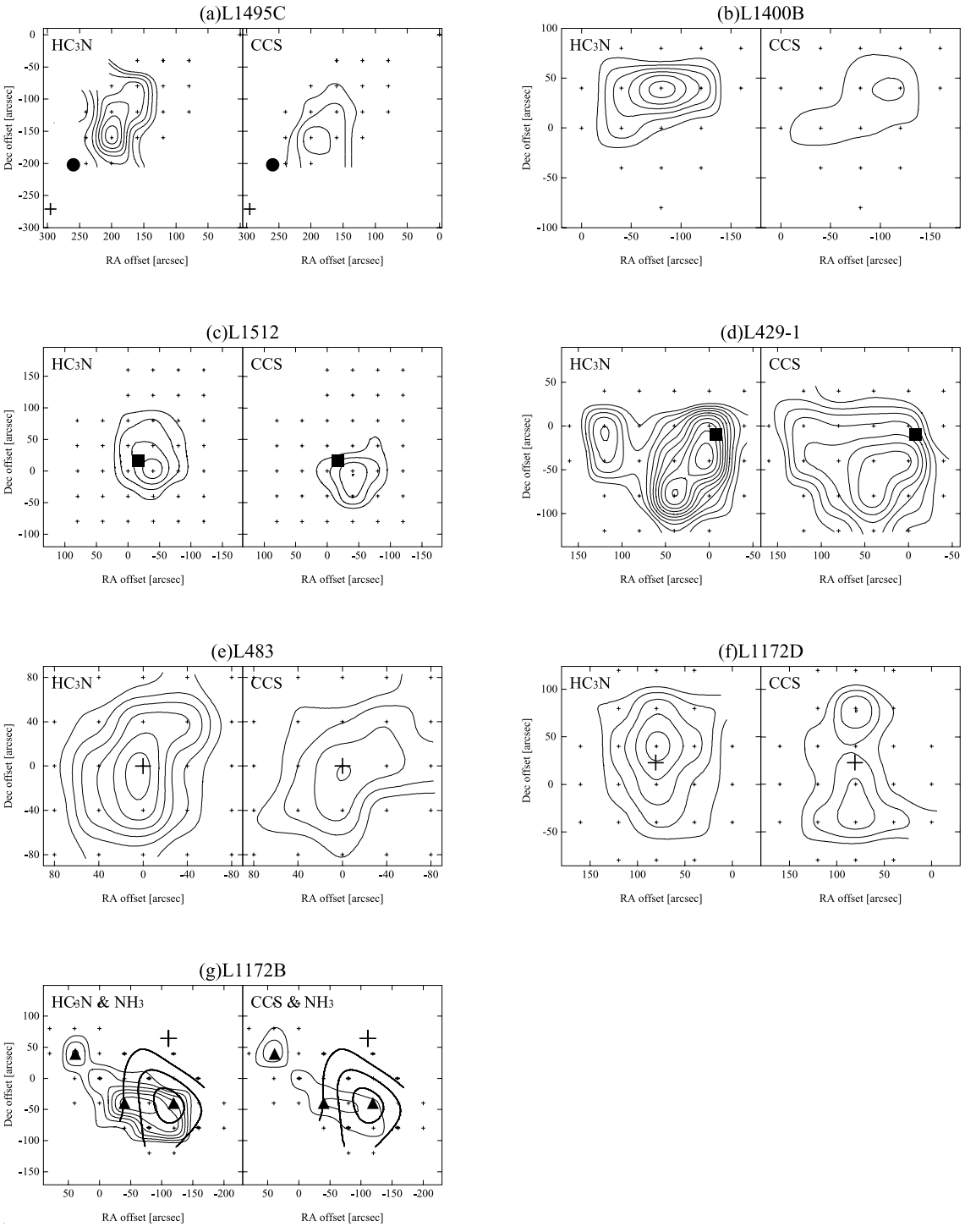


Fig. 4.— Integrated intensity maps of $HC_3N$ and CCS. (a) L1495C. A cross indicates the *IRAS* source (*IRAS* 04018+2803) and a filled circle represents the position of the $NH_3$ peak of L1495N (Benson & Myers 1989). *Left:* $HC_3N(J$=5-4). The velocity range of integration is 5.7-7.1 km $s^{-1}$. The interval of the contours is 0.1 K km $s^{-1}$ and the lowest one is 0.3 K km $s^{-1}$. *Right:* $CCS(J_N$=$4_3$-$3_2)$. The velocity range of integration is 5.7-6.9 km $s^{-1}$. The interval of the contours is 0.1 K km $s^{-1}$ and the lowest one is 0.3 K km $s^{-1}$. (b) L1400B. *Left:* $HC_3N(J$=5-4). The velocity range of integration is 2.8-4.0 km $s^{-1}$. The interval of the contours is 0.05 K km $s^{-1}$ and the lowest one is 0.15 K km $s^{-1}$. *Right:* $CCS(J_N$=$4_3$-$3_2)$. The velocity range of integration is 2.8-3.7 km $s^{-1}$. The interval of the contours is 0.05 K km $s^{-1}$

and the lowest one is 0.15 K km $s^{-1}$. (c) L1512. A filled square represents the peak position of the dust continuum emission (Kirk et al. 2005). *Left:* $HC_3N$($J$=5-4). The velocity range of integration is 6.5-7.8 km $s^{-1}$. The interval of the contours is 0.2 K km $s^{-1}$ and the lowest one is 0.6 K km $s^{-1}$. *Right:* CCS($J_N$=$4_3$-$3_2$). The velocity range of integration is 6.6-7.7 km $s^{-1}$. The interval of the contours is 0.05 K km $s^{-1}$ and the lowest one is 0.15 K km $s^{-1}$. (d) L429-1. A filled square represents the peak position of the dust continuum emission (Crapsi et al. 2005). *Left:* $HC_3N$($J$=5-4). The velocity range of integration is 6.0-7.7 km $s^{-1}$. The interval of the contours is 0.05 K km $s^{-1}$ and the lowest one is 0.15 K km $s^{-1}$. *Right:* CCS($J_N$=$4_3$-$3_2$). The velocity range of integration is 6.3-7.5 km $s^{-1}$. The interval of the contours is 0.05 K km $s^{-1}$ and the lowest one is 0.15 K km $s^{-1}$. (e) L483. A cross indicates the *IRAS* source (*IRAS* 18148-0440). *Left:* $HC_3N$($J$=5-4). The velocity range of integration is 4.5-6.5 km $s^{-1}$. The interval of the contours is 0.2 K km $s^{-1}$ and the lowest one is 0.6 K km $s^{-1}$. *Right:* CCS($J_N$=$4_3$-$3_2$). The velocity range of integration is 4.8-6.0 km $s^{-1}$. The interval of the contours is 0.07 K km $s^{-1}$ and the lowest one is 0.21 K km $s^{-1}$. (f) L1172D. A cross indicates the *IRAS* source (*IRAS* 21017+6742). *Left:* $HC_3N$($J$=5-4). The velocity range of integration is 2.0-4.0 km $s^{-1}$. The interval of the contours is 0.2 K km $s^{-1}$ and the lowest one is 0.6 K km $s^{-1}$. *Right:* CCS($J_N$=$4_3$-$3_2$). The velocity range of integration is 2.2-3.5 km $s^{-1}$. The interval of the contours is 0.05 K km $s^{-1}$ and the lowest one is 0.15 K km $s^{-1}$. (g) L1172B. A cross indicates the *IRAS* source (*IRAS* 21025+6801). The three positions toward which the molecular abundances are obtained, (-120″,-40″), (-40″,-40″), and (+40″,+40″), are indicated by filled triangles. Bold contours represent the integrated intensity map of the $NH_3$ (1,1) lines with their interval and the lowest level are 0.044 K km $s^{-1}$ and 0.132 K km $s^{-1}$, respectively. *Left:* $HC_3N$($J$=5-4). The velocity range of integration is 1.6-3.6 km $s^{-1}$. The interval of the contours is 0.07 K km $s^{-1}$ and the lowest one is 0.21 K km $s^{-1}$. *Right:* CCS($J_N$=$4_3$-$3_2$). The velocity range of integration is 1.8-3.3 km $s^{-1}$. The interval of the contours is 0.05 K km $s^{-1}$ and the lowest one is 0.15 K km $s^{-1}$.

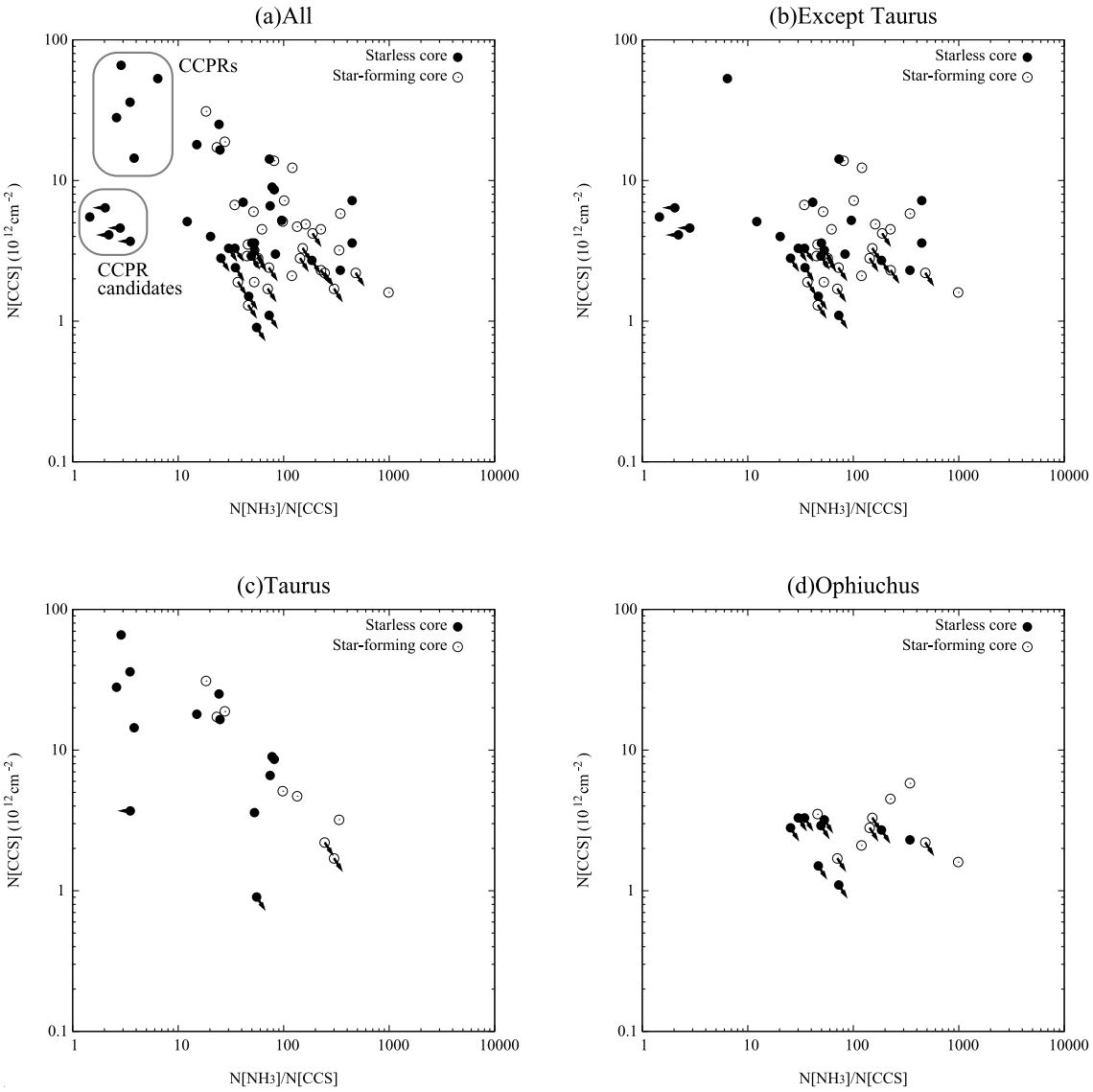


Fig. 5.— Relationships between the $NH_3$/CCS ratios and the column densities of CCS. The cores where either CCS or $NH_3$ are detected are plotted. Filled and open symbols represent the cores without *IRAS* sources (starless cores) and the cores with *IRAS* sources (star-forming cores), respectively. Arrows represent the upper or lower limit of the values. (a) All samples listed in Table A.1. (b) Same as (a) but except for Taurus cores. (c) Taurus cores. (d) Ophiuchus cores.

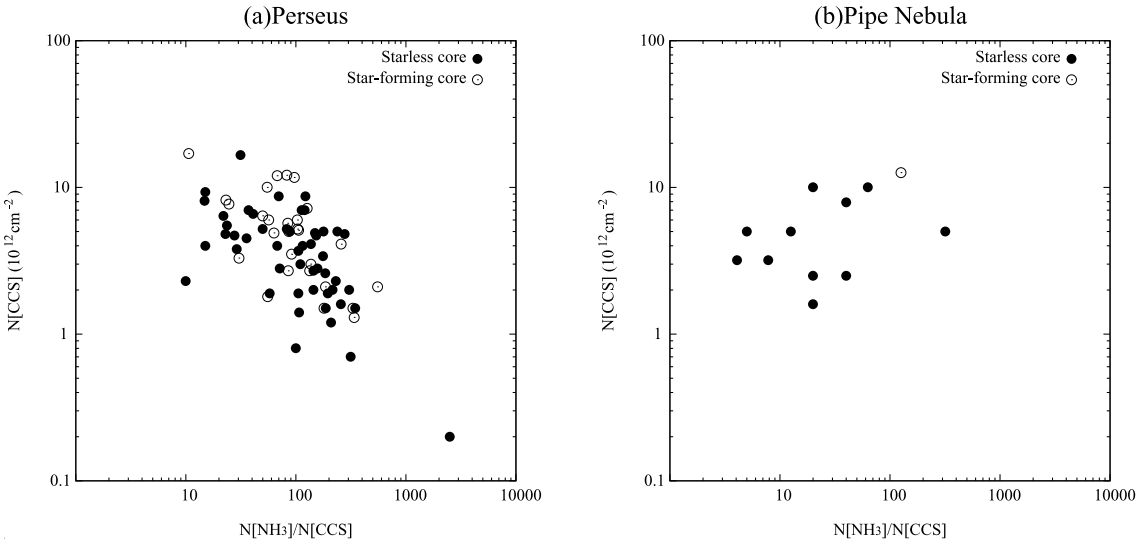


Fig. 6.— Relationships between the $NH_3$/CCS ratios and the column densities of CCS. (a) Perseus cores. The star-forming cores are identified according to Enoch et al. (2006), which are labeled as "Bolocam" sources in Rosolowsky et al. (2008). We tentatively regard the sources other than "Bolocam" in Rosolowsky et al. (2008) as the starless cores. Only the cores where both CCS and $NH_3$ are detected are plotted. (b) Pipe cores. In this panel, we indicated the Pipe core 12 as the only the site of star-formation (Brooke et al. 2007). Only the cores where both CCS and $NH_3$ are detected are shown.

## A. Individual Sources

In this appendix, we will describe the individual sources where at least one of the observed lines were detected.

### A.1. L1495C

This core, taken from Benson & Myers (1989), is a starless core located in the Taurus molecular cloud at a distance of 137 pc (Torres et al. 2007). We first detected the CCS and $HC_3N$ lines at the (+80″, -80″) position in right ascension and declination, respectively, with respect to the reference position of L1495C. Then we extended our maps to about 4′ southeast from the reference position, and found that the peak positions of CCS and $HC_3N$ are located within the $NH_3$ core of L1495N observed by Benson & Myers (1989). Its position offset is (-60″,+42″) with respect to the reference position of L1495N. Therefore, the CCS and $HC_3N$ cores detected in the present study should be referred to L1495N rather than L1495C. The integrated intensity maps for CCS and $HC_3N$ are shown in Figure 4(a). The *IRAS* source and the $NH_3$ core are located at the southeast edge of our map. Because the CCS and $HC_3N$ peaks correspond to the northwestern edge of the $NH_3$ core of L1495N (Benson & Myers 1989), the carbon-chain molecules seem to be depleted at the $NH_3$ peak of L1495N.

### A.2. L1400B

This core is one of the starless cores listed in Benson & Myers (1989), whose distance is 170 pc (Hilton & Lahulla 1995). We detected the CCS and $HC_3N$ lines toward the (-80″, +40″) northwest from the reference position. The integrated intensity maps for CCS and $HC_3N$ are shown in Figure 4(b). The peak position of CCS may be shifted from that of $HC_3N$, although it is unclear due to the low signal-to-noise ratio and the coarse sampling. We also detected the $NH_3$ lines toward the (-80″, +40″) position. Because the $NH_3$ lines were not detected by Benson & Myers (1989), this is the first detection of the $NH_3$ lines toward L1400B. The line parameters are listed in Table 4.

### A.3. L1527

A dense core associated with L1527 in the Taurus molecular cloud is a host of Class 0 protostar *IRAS* 04368+2557, which is listed in Benson & Myers (1989). The CCS line was detected in previous observations (Hirota et al. 2001). Recently, Sakai et al. (2008a) detected the lines of various carbon-chain molecules such as $C_nH$ ($n$=4,5,6) and $C_nH_2$ ($n$=3,4,6) in this source. Because of their high excitation temperature (>10 K), Sakai et al. (2008a) proposed a different type of carbon-chain chemistry other than that in the cold dark cloud cores, and called it as Warm Carbon-Chain Chemistry (WCCC). The column density of $HC_5N$ listed in Table 5 is 3.5 times larger than that of Sakai et al. (2008a) due to a difference in the

assumed excitation temperature (6.5 K); Sakai et al. (2008a) employed a higher excitation temperature of 12.3 K by assuming that the line mainly comes from a dense and warm part near the protostar. Since we observed a single transition for each molecule only toward the *IRAS* position, it is not possible from our data to discuss molecular distribution and their excitation condition in detail.

### A.4. L1517D

L1517D is a starless dense core in the Taurus molecular cloud (Benson & Myers 1989). We searched for the molecular lines around the reference position. The CCS line was detected only toward the (+80″, +80″) position, while the $HC_3N$ and $HC_5N$ lines were not detected toward all the observed positions, as shown in Figure 3(a). The $NH_3$ line was detected neither toward the reference position (Benson & Myers 1989) nor the CCS position above, suggesting that L1517D would be one of the new candidates for CCPRs with an extremely low $NH_3$/CCS ratio. On the other hand, it would be possible that the weak CCS emission and the low $NH_3$/CCS ratio are due to the offset from the core center, as in the case of L1498 and L1544 where the CCS lines tend to be intense at the outer part of the dense cores (Kuiper et al. 1996; Ohashi et al. 1999). In L1517D, the position where the CCS line was detected corresponds to the edge of the *Spitzer* 160 $\mu$m continuum emission image with the 40″ resolution (Kirk et al. 2007), although the dense core is not detected in the higher resolution observations with SCUBA. Further high resolution mapping observations of both dust continuum emission and molecular lines are required to confirm whether L1517D is one of the CCPRs.

### A.5. L1512

L1512 is one of the well studied starless dense cores in the Taurus molecular cloud (Benson & Myers 1989). Since the CCS, $HC_3N$, and $HC_5N$ lines were detected in the previous observations (Suzuki et al. 1992), we carried out mapping observations of the CCS and $HC_3N$ lines in the present study. The results are shown in Figure 4(c). The derived column densities of CCS and $HC_3N$ are larger than those reported by Suzuki et al. (1992) because the peak positions of CCS and $HC_3N$ are significantly shifted from the reference position (Suzuki et al. 1992). The position of the dust continuum emission is plotted in Figure 4(c) (Kirk et al. 2005). We found that the integrated intensity maps of CCS and $HC_3N$ do not show a central hole, which is consistent with the results by Lee et al. (2003). However, their peak positions are shifted from the dust continuum peak by (-24″, -17″) in right ascension and declination, respectively. In particular, the CCS emission traces the southwest edge of the dust continuum emission, possibly suggesting the depletion of CCS at the dust continuum peak.

### A.6. L183(N)

L183 is a well studied dark cloud, which is also known as L134N, and L183(N) is one of the ammonia cores in the filamentary dense molecular cloud L183 (Ungerechts et al. 1980; Benson & Myers 1989). The estimated distance of L183 is about 140 pc, although some other results are also reported (Hilton & Lahulla 1995). The CCS lines were observed previously by Benson et al. (1998). We observed only toward one position, which corresponds to the position for the DNC and $HN^{13}C$ observations (Hirota et al. 2001). The column density of CCS derived for this position agrees well with the previous result (Benson et al. 1998).

### A.7. B68

B68 is a dense starless core located in the Pipe Nebula at an estimated distance of 130-200 pc (Hilton & Lahulla 1995; Rathborne et al. 2008). We detected the CCS, $HC_3N$, and $HC_5N$ lines toward the reference position, although we could not carry out the mapping observations due to the limited observing time. The CCS and $NH_3$ maps were presented by Lai et al. (2003). In our study, the column density is derived toward the $NH_3$ peak, which is offset by 45″ from the CCS peak (Lai et al. 2003), so that the derived column density of CCS is different from that of Lai et al. (2003), by a factor of 2-3.

### A.8. L492

L492 is a Bok globule located in the Aquila rift at a distance of 200 pc (Lee & Myers 1999). This core was not listed in the $NH_3$ survey by Benson & Myers (1989), while we included it in our survey because an intense CS line was detected toward this source (Lee et al. 2001). In the initial survey observations conducted in 2002, we found that the CCS, $HC_3N$, and $HC_5N$ lines toward the reference position of L492 are extremely strong. Therefore, we carried out follow-up mapping observations of L492 in various molecular lines. Further details were reported in Hirota & Yamamoto (2006).

### A.9. L429-1

L429-1 is also a Bok globule located in the Aquila rift at a distance of 200 pc (Lee & Myers 1999). Similar to L492, this core was not included in the $NH_3$ survey by Benson & Myers (1989), while we observed it based on the results of the CS survey by Lee et al. (2001). Because intense CCS and $HC_3N$ lines were detected toward the reference position of L429-1, we carried out mapping observations of the CCS and $HC_3N$ lines. The results are shown in Figure 4(d). The overall structures seen in the integrated intensity maps of CCS and $HC_3N$ are similar, while the $HC_3N$ map shows relatively complex clumpy structure. There seem to be three cores in our map. According to the dust continuum observations (Crapsi et al. 2005), the CCS and $HC_3N$ distributions are significantly shifted from the continuum peak position, although the mapped region of the dust continuum emission (Crapsi et al. 2005)

is limited to the northwestern peak of the CCS and $HC_3N$ cores. For much wider area, the mid-infrared absorption map is available. It shows an extended high extinction region toward east of the dust continuum peak (Bacmann et al. 2000), which agrees well with the $HC_3N$ and CCS maps. Another peak of $HC_3N$ and the weak emission of the CCS lines can be seen toward 150″ east of the dust continuum peak. We observed the $NH_3$ line only toward the reference position of L429-1, and hence, the $NH_3$/CCS ratio at the eastern peak of $HC_3N$, is not calculated. In spite of the intense $HC_3N$ emission, the $HC_5N$ line was not detected in L429-1.

### A.10. L483

L483 is a star-forming dense core in the Aquila rift at a distance of 200 pc (Hilton & Lahulla 1995). An intense CCS line was detected by Benson et al. (1998). We derived the column density which is consistent with that of Benson et al. (1998). We also detected intense $HC_3N$ and $HC_5N$ lines toward the reference position of L483 as shown in Figure 2. Then, we carried out mapping observations in the $HC_3N$ and CCS lines. The results are shown in Figure 4(e). According to the previous observations of molecular lines and submillimeter continuum emission (Fuller et al. 1995), L483 harbors a Class 0 protostar IRAS 18148-0440 associated with molecular outflows. The CCS and $HC_5N$ lines are quite strong toward the central protostar, although we cannot completely rule out the possibility that these centrally peaked structure would be an artifact due to insufficient spatial resolution, as seen in Velusamy et al. (1995). Extremely high abundances of carbon-chain molecules toward the Class 0 protostar are apparently similar to the L1527 core (Sakai et al. 2008a), and are indicative of WCCC (Sakai et al. 2009). However, higher abundance of CCS than that in L1527 seems to be rather common characteristics for CCPRs such as L1495B, L1521B, L1521E and the cyanopolyyne peak of TMC-1 (Hirota et al. 2002, 2004). Observations of higher excitation lines of carbon-chain molecules in L483 would be crucial to distinguish whether L483 is categorized as WCCC or CCPR.

### A.11. L530D

L530D is a dense core which is included in the survey of $NH_3$ by Benson & Myers (1989). The estimated distance is 350 pc (Hilton & Lahulla 1995). We searched for the lines around the reference position of L530D, and found that the peak position of the CCS line is located at (+80″, +40″). However, the $HC_3N$ and $HC_5N$ lines were not detected toward this position, as shown in Figures 3(b). This position is offset by 85″ northeast of the dust continuum peak (Kirk et al. 2005). On the other hand, the $NH_3$ line was detected toward the dust continuum peak (Benson & Myers 1989; Kirk et al. 2005), while it was not detected toward the CCS peak in our observations. Although the $NH_3$/CCS ratio at the CCS peak in L530D is as low as those of the other CCPRs, lower column densities of CCS and other carbon-chain molecules, the offsets of the CCS peak from the dust continuum emission, and the detection of $NH_3$ at the dust continuum peak would suggest that the CCS line traces the outer part of this core, similar to the case of L1517D. In fact, the column density of $NH_3$ toward the dust

continuum peak is derived to be $7.9\times10^{13}$ cm$^{-2}$ from the data of Benson & Myers (1989), which results in the $NH_3$/CCS ratio toward the dust continuum peak 10 times larger than that toward the CCS peak. Molecular distributions in L530D seem to be similar to those in L1498 and L1544, where the $NH_3$ peak is coincident with the dust continuum and CCS is distributed in the surrounding region (Kuiper et al. 1996; Ohashi et al. 1999). However, we cannot totally rule out the possibility that L530D is a candidate for the CCPR because of a lack of complete mapping observations in the CCS and $NH_3$ lines.

### A.12. L1147

L1147 is a dense core located in the Cepheus region at a distance of 325 pc (Hilton & Lahulla 1995). This source is included in the survey of the $NH_3$ lines (Benson & Myers 1989). We searched for the CCS, $HC_3N$, and $HC_5N$ lines around the reference position of L1147, and detected the CCS and $HC_3N$ lines only toward the (0″, -80″) position, whose spectra are shown in Figures 3(c). The $HC_5N$ line was not detected toward all the observed position. The $NH_3$ line was detected toward both the reference position (Benson & Myers 1989) and the CCS peak. The position of the CCS peak is offset by only 20″ toward south of the dust continuum peak of L1148, which is 1′ south of L1147 (Myers et al. 1983; Kirk et al. 2005), and hence, the dense core of L1147 found in the present survey can be regarded as L1148. The relatively low $NH_3$/CCS ratio toward the dust continuum peak of L1147 means that it could be a candidate for the CCPR.

### A.13. L1172D

L1172D was originally identified as a starless dense core in the survey of the $NH_3$ lines (Benson & Myers 1989), which is located in the Cepheus region at a distance of 288 pc (Hilton & Lahulla 1995). At first, the CCS and $HC_3N$ lines were found to be intense toward the eastern part of the core of L1172D, and hence, the mapping region was extended toward 1′-2′ east from the reference position. Then the CCS and $HC_3N$ emission peaks were found to be located toward L1172A, another star-forming dense core identified by Benson & Myers (1989). There is a Class I protostar, *IRAS* 21017+6742, at the center of the core, which is known to be an engine of the molecular outflow (Myers et al. 1988). The integrated intensity maps for $HC_3N$ and CCS are shown in Figure 4(f). The $HC_3N$ peak corresponds to the *IRAS* position, while CCS is significantly depleted toward the center of the $HC_3N$ core. The shape and size of the $HC_3N$ core is quite similar to that of $NH_3$ (Benson & Myers 1989). These results suggest that CCS is depleted as in the case of B335 (Velusamy et al. 1995), while $HC_3N$ is abundant toward the central part of the core.

### A.14. L1172B

L1172B is also identified as a starless dense core in the Cepheus region, which is observed in the survey of the $NH_3$ lines (Benson & Myers 1989). The observed spectra toward three

positions in L1172B and the integrated intensity maps for $HC_3N$ and CCS are shown in Figures 3(d)-(f) and 4(g), respectively. A dense core traced by the CCS and $HC_3N$ lines shows an elongated structure extending from northeast to southwest, and consists of at least two clumps. The integrated intensity map of the $NH_3$ lines is also shown in Figure 4(g) in thick contour lines. The $NH_3$ lines are detected only toward the western edge of the elongated molecular cloud core traced by the CCS and $HC_3N$ lines. The $NH_3$/CCS abundance ratios are relatively low in the northeast clump, (+40″, +40″), and hence, this clump can be a candidate of CCPR. An *IRAS* point source, *IRAS* 21025+6801, is located at northwest of the core, although it is not clear whether this source is physically associated with the core of L1172B.

### A.15. L183(S), L1696A, L1689N, L1157, L1155C, and L1228

The results of the CCS observations have already been reported for these sources (Hirota et al. 2001). We reanalyzed the $HC_3N$ data for these sources, while we did not make further observations of the $HC_5N$ lines.

## B. Compilation of the samples of the CCS and $NH_3$ cores

As mentioned in Introduction, several survey observations of the CCS and $NH_3$ lines (Benson & Myers 1989; Fuente et al. 1990; Suzuki et al. 1992; Scappini & Codella 1996; Benson et al. 1998; Turner et al. 1998; Lai & Crutcher 2000; Hirota et al. 2001; de Gregorio-Monsalvo et al 2006; Rathborne et al. 2008; Rosolowsky et al. 2008; Sakai et al. 2008b; Tatematsu et al. 2008) were carried out for the nearby molecular clouds. Here we compiled the results for CCS, as listed in Table A.1. In this paper, we mainly focused on results of the observations of the CCS lines toward the nearby molecular cloud cores conducted with the single dish telescope in the 45 GHz band (Suzuki et al. 1992; Benson et al. 1998; Hirota et al. 2001) to compare with the present results, all of which are analyzed by almost the same methods.

### B.1. CCS samples

For the statistical study with uniform samples of nearby dark cloud cores, we excluded results of other surveys which were conducted in the different frequency bands and/or with interferometers (Scappini & Codella 1996; Lai & Crutcher 2000; de Gregorio-Monsalvo et al. 2006; Rathborne et al. 2008; Rosolowsky et al. 2008), while we referred to the results by Rathborne et al. (2008) and Rosolowsky et al. (2008) for comparison of source-to-source variation of molecular abundances. We only employed dark cloud cores and low-mass star-forming regions in our sample as uniformly as possible. As a result, some of the sources in the high-mass star-forming molecular clouds in the Orion region (e.g., Tatematsu et al. 2008) were not included in our samples. We also excluded the different kind of samples such as translucent clouds (Turner et al. 1998) and distant infrared dark clouds (Sakai et al. 2008b). For a similar reason, we did not include the results of individual sources (e.g., Velusamy et al.

1995; Kuiper et al. 1996; Ohashi et al. 1999; Lai et al. 2003; Lee et al. 2003), although these sources are included in the part of the survey observations. For the sources which are included in more than two literatures, we adopted one of the results as indicated in Table A.1 to avoid overlap of the samples. As a result, our sample consists of 90 nearby dark cloud cores as listed in Table A.1.

We compared the results of several sources which are observed both in our observations and previous ones, such as L1527, L1512, L1523, L183(N), L1719B, B68, L483, and L1172A (L1172D) (Suzuki et al. 1992; Benson et al. 1998; Hirota et al. 2001; Lai et al. 2003). As a result, we found that the difference in the derived column density is typically within 40% but is a factor of 3 in the worst case, which is mostly due to the difference in the observed position (e.g., in the case of L1512; Suzuki et al. 1992; Benson et al. 1998). These uncertainties are comparable to those attributed to the unknown excitation temperatures as already discussed in the main text.

### B.2. $NH_3$ samples

For the $NH_3$ lines, substantial amount of the sources listed in Table A.1 were observed by Benson & Myers (1989). However, the column densities of $NH_3$ were reported for a part of the sources where the intense spectra were detected. Therefore, we calculated the column densities of $NH_3$ lines using the line parameters reported by Benson & Myers (1989). The method is described by Suzuki et al. (1992), in which we assumed the excitation temperature of 6.5 K. If the $NH_3$ lines were not detected, we calculated the upper limits for the column densities by assuming the line width of 0.5 km $s^{-1}$.

The data for the $NH_3$ lines are mostly taken from the systematic survey observations by Benson & Myers (1989) and Suzuki et al. (1992), while some individual observations are included (Ungerechts et al. 1980; Mundy et al. 1990; Bachiller et al. 1993; Ladd et al. 1994; Anglada et al. 1997; Hirota et al. 2002, 2004). Therefore, the uncertainties in the column densities of $NH_3$ might be affected by the difference in the observations and data analysis such as the telescope beam sizes and assumed and/or derived kinetic temperatures. However, we estimate that the uncertainties in the column densities of $NH_3$ is within a factor of 2 for most of the sources as discussed in Suzuki et al. (1992).

Table A.1. Summary of Column Densities of CCS, $HC_3N$, $HC_5N$, and $NH_3$

| Source | | | | YSO(*IRAS*) | | Distance | | $N$[CCS] | $N$[$HC_3N$] | $N$[$HC_5N$] | $N$[$NH_3$] | |
|---|---|---|---|---|---|---|---|---|---|---|---|---|
| No | Name | RA(J2000) | Dec(J2000) | Name | Region | (pc) | Ref. | ($10^{12}$ cm$^{-2}$) | ($10^{12}$ cm$^{-2}$) | ($10^{12}$ cm$^{-2}$) | ($10^{14}$ cm$^{-2}$) | Ref. |
| 1 | L1455 | 03 27 40.3 | +30 13 03 | L1455-FIR4 | Perseus | 235 | 1 | 7.2 | 3.6 | <3.8 | 7.3 | 1,1,1,1 |
| 2 | Per5 | 03 29 51.6 | +31 39 04 | 03267+3128 | Perseus | 235 | 1 | 1.9 | ··· | ··· | 1.0 | 2,*,*,3 |
| 3 | B1 | 03 33 16.3 | +31 07 51 | 03301+3057 | Perseus | 235 | 1 | 13.8 | 8.5 | 8.8 | 11.2 | 1,1,1,1 |
| 4 | B5 | 03 47 38.4 | +32 52 43 | 03445+3242 | Perseus | 235 | 1 | 6.7 | 6.8 | <2.8 | 2.3 | 1,1,1,1 |
| 5 | L1489 | 04 04 50.6 | +26 19 41 | 04016+2610 | Taurus | 137 | 2 | 4.7 | 12.8 | 5.8 | 6.3 | 1,1,1,1 |
| 6 | L1498 | 04 10 51.5 | +25 09 58 | ··· | Taurus | 137 | 2 | 16.5 | 15.8 | 4.3 | 4.1 | 1,1,1,1 |
| 7 | L1495C/L1495N | 04 13 45.7 | +28 13 14 | 04108+2803 | Taurus | 137 | 2 | 17.2 | 13.8 | <9.0 | 4.0 | 4,4,4,5 |
| 8 | L1495 | 04 14 12.1 | +28 09 30 | 04108+2803 | Taurus | 137 | 2 | <1.7 | 4.6 | <3.2 | 5.1 | 1,1,1,1 |
| 9 | L1495D | 04 14 18.2 | +28 15 52 | ··· | Taurus | 137 | 2 | <2.2 | <1.4 | <4.9 | <1.0 | 4,4,4,5 |
| 10 | L1495B | 04 15 36.5 | +28 47 06 | ··· | Taurus | 137 | 2 | 14.4 | 21 | 5.2 | 0.55 | 6,6,6,6 |
| 11 | L1506 | 04 18 31.1 | +25 19 25 | ··· | Taurus | 137 | 2 | <2.8 | <1.7 | <6.2 | <0.5 | 4,4,4,5 |
| 12 | L1521C | 04 19 19.2 | +27 16 29 | ··· | Taurus | 137 | 2 | <1.1 | <0.7 | <2.5 | <0.3 | 1,1,1,1 |
| 13 | L1521B | 04 24 12.7 | +26 36 53 | ··· | Taurus | 137 | 2 | 36 | 41 | 12 | 1.26 | 6,6,6,6 |
| 14 | L1400B | 04 24 37.3 | +55 02 33 | ··· | other | 170 | 3 | 5.1 | 5.0 | <5.3 | 0.62 | 4,4,4,4 |
| 15 | L1521A | 04 26 43.9 | +26 15 48 | ··· | Taurus | 137 | 2 | <0.9 | <0.7 | <2.0 | <0.3 | 1,1,1,1 |
| 16 | L1521D | 04 27 46.5 | +26 17 52 | ··· | Taurus | 137 | 2 | 3.6 | 1.2 | <2.0 | 1.9 | 1,1,1,1 |
| 17 | L1400E | 04 28 28.5 | +54 47 36 | ··· | other | 170 | 3 | <2.6 | <1.6 | <5.6 | <0.82 | 4,4,4,5 |
| 18 | L1521E | 04 29 16.5 | +26 13 50 | ··· | Taurus | 137 | 2 | 28 | 23 | 4.6 | 0.73 | 7,7,7,7 |
| 19 | L1400F | 04 29 51.4 | +54 14 19 | ··· | other | 170 | 3 | <2.4 | <1.6 | <5.1 | 0.84 | 4,4,4,5 |
| 20 | L1400K | 04 30 52.1 | +54 51 55 | ··· | other | 170 | 3 | 3.6 | 6.4 | <2.3 | 1.8 | 1,1,1,1 |
| 21 | L1551A | 04 30 58.1 | +18 17 10 | ··· | Taurus | 137 | 2 | <2.6 | <1.5 | <5.5 | <0.98 | 4,4,4,5 |
| 22 | L1551 | 04 31 30.0 | +18 12 30 | 04287+1806 | Taurus | 137 | 2 | <2.3 | <1.4 | <5.0 | <0.72 | 4,4,4,5 |
| 23 | L1551S | 04 31 33.9 | +18 08 05 | 04287+1801 | Taurus | 137 | 2 | <2.2 | 6.2 | <1.8 | 5.4 | 1,1,1,1 |
| 24 | TMC-2A | 04 31 55.9 | +24 32 49 | 04292+2422 | Taurus | 137 | 2 | 3.2 | 3.7 | <1.6 | 10.7 | 1,1,1,1 |
| 25 | L1445 | 04 32 07.0 | +46 37 23 | ··· | other | ··· | ··· | <2.3 | <1.6 | <5.3 | ··· | 4,4,4,* |
| 26 | TMC-2 | 04 32 44.8 | +24 25 12 | ··· | Taurus | 137 | 2 | 25 | 33 | 6.7 | 6.1 | 1,1,1,1 |
| 27 | L1536B | 04 33 25.6 | +22 43 26 | ··· | Taurus | 137 | 2 | 6.6 | 5.7 | <2.6 | 4.9 | 1,1,1,1 |
| 28 | L1527 | 04 39 53.6 | +26 03 05 | 04368+2557 | Taurus | 137 | 2 | 5.1 | 47 | 18.9 | 5.0 | 8,4,4,5 |
| 29 | TMC-1($NH_3$) | 04 41 23.0 | +25 48 13 | 04381+2540 | Taurus | 137 | 2 | 18.8 | 61 | 10.0 | 5.2 | 1,1,1,1 |
| 30 | TMC-1C | 04 41 34.3 | +26 00 43 | 04385+2550 | Taurus | 137 | 2 | 31 | 28 | 9.4 | 5.7 | 1,1,1,1 |
| 31 | TMC-1(CP) | 04 41 42.5 | +25 40 42 | ··· | Taurus | 137 | 2 | 66 | 171 | 56 | 1.9 | 1,1,1,1 |
| 32 | L1517C | 04 54 42.8 | +30 34 48 | ··· | Taurus | 137 | 2 | <1.1 | <0.7 | <1.9 | <0.3 | 1,1,1,1 |
| 33 | L1517A | 04 55 06.3 | +30 33 40 | ··· | Taurus | 137 | 2 | <0.9 | <0.7 | <1.9 | 0.5 | 1,1,1,1 |
| 34 | L1517B | 04 55 18.8 | +30 38 04 | ··· | Taurus | 137 | 2 | 8.6 | 9.3 | 4.3 | 7.0 | 1,1,1,1 |

Table A.1—Continued

| No | Source Name | RA(J2000) | Dec(J2000) | YSO(*IRAS*) Name | Region | Distance (pc) | Ref. | $N$[CCS] ($10^{12}$ cm$^{-2}$) | $N$[$HC_3N$] ($10^{12}$ cm$^{-2}$) | $N$[$HC_5N$] ($10^{12}$ cm$^{-2}$) | $N$[$NH_3$] ($10^{14}$ cm$^{-2}$) | Ref. |
|---|---|---|---|---|---|---|---|---|---|---|---|---|
| 35 | L1517D | 04 55 54.4 | +30 40 05 | ··· | Taurus | 137 | 2 | 3.7 | <1.1 | <3.7 | <0.13 | 4,4,4,4 |
| 36 | L1512 | 05 04 06.5 | +32 43 09 | ··· | Taurus | 137 | 2 | 9.0 | 25 | <2.1 | 7.0 | 4,4,1,1 |
| 37 | L1544 | 05 04 15.2 | +25 11 08 | ··· | Taurus | 137 | 2 | 18.0 | 17.8 | 7.8 | 2.7 | 1,1,1,1 |
| 38 | L1523 | 05 06 22.9 | +31 41 19 | ··· | Taurus | 137 | 2 | <2.2 | <1.4 | <4.8 | <1.06 | 4,4,4,5 |
| 39 | L1778A | 15 39 27.5 | −07 10 08 | ··· | other | 100 | 3 | <3.0 | <1.6 | <6.3 | <1.03 | 4,4,4,5 |
| 40 | L183(N) | 15 54 09.2 | −02 49 42 | ··· | other | 140 | 3 | 3.6 | 13.7 | <7.3 | 16 | 4,4,4,9 |
| 41 | L183(S) | 15 54 09.2 | −02 51 39 | ··· | other | 140 | 3 | 7.2 | 4.1 | ··· | 32 | 8,4,*,9 |
| 42 | L1721 | 16 14 28.2 | −18 54 44 | ··· | Ophiuchus | 120 | 4 | <3.1 | <1.8 | <7.0 | <0.81 | 4,4,4,5 |
| 43 | L1719B | 16 22 12.4 | −19 38 41 | ··· | Ophiuchus | 120 | 4 | <3.3 | <1.8 | <7.0 | <0.87 | 4,4,4,5 |
| 44 | L1687 | 16 23 01.6 | −22 53 41 | ··· | Ophiuchus | 120 | 4 | <1.5 | <0.8 | <2.6 | <0.3 | 1,1,1,1 |
| 45 | L1681A | 16 26 26.6 | −24 33 16 | ··· | Ophiuchus | 120 | 4 | <2.4 | <1.0 | <3.4 | <0.4 | 1,1,1,1 |
| 46 | L1681B | 16 27 26.9 | −24 44 27 | 16244-2432 | Ophiuchus | 120 | 4 | <1.7 | <1.0 | <3.2 | 1.2 | 1,1,1,1 |
| 47 | L1690 | 16 27 46.4 | −24 16 59 | ··· | Ophiuchus | 120 | 4 | <3.1 | <1.8 | <7.0 | <0.72 | 4,4,4,5 |
| 48 | L1696A | 16 28 31.5 | −24 19 08 | ··· | Ophiuchus | 120 | 4 | <2.7 | <2.1 | <2.0 | 5.0 | 8,4,10,5 |
| 49 | L1696B | 16 29 03.0 | −24 21 33 | ··· | Ophiuchus | 120 | 4 | <1.3 | <0.8 | <2.3 | <0.3 | 1,1,1,1 |
| 50 | L1709A | 16 30 50.8 | −23 41 03 | ··· | Ophiuchus | 120 | 4 | <3.3 | <1.8 | <7.2 | 0.99 | 4,4,4,5 |
| 51 | L1709B | 16 31 39.6 | −24 01 23 | 16285-2356 | Ophiuchus | 120 | 4 | 3.5 | 5.9 | <2.3 | 1.6 | 1,1,1,1 |
| 52 | L1689A | 16 32 12.6 | −25 02 53 | ··· | Ophiuchus | 120 | 4 | <3.2 | <1.7 | <4.8 | 1.7 | 1,1,1,1 |
| 53 | L1689N | 16 32 22.8 | −24 28 33 | 16293-2422 | Ophiuchus | 120 | 4 | 5.8 | 7.5 | ··· | 20 | 8,4,*,11 |
| 54 | $\rho$-Oph-E | 16 32 29.5 | −24 28 13 | 16293-2422 | Ophiuchus | 120 | 4 | <2.2 | 4.3 | <2.8 | 10.6 | 1,1,1,1 |
| 55 | L1709C | 16 33 53.4 | −23 38 32 | ··· | Ophiuchus | 120 | 4 | <3.3 | <1.7 | <6.9 | 1.14 | 4,4,4,5 |
| 56 | L1709 | 16 34 36.0 | −23 43 11 | ··· | Ophiuchus | 120 | 4 | <1.5 | <0.9 | <2.7 | 0.7 | 1,1,1,1 |
| 57 | L43E | 16 34 39.8 | −15 47 00 | 16316-1540 | Ophiuchus | 120 | 4 | 4.5 | 3.7 | <1.8 | 10.1 | 1,1,1,1 |
| 58 | L1689B | 16 34 42.1 | −24 36 11 | ··· | Ophiuchus | 120 | 4 | <1.1 | <0.8 | <1.9 | 0.8 | 1,1,1,1 |
| 59 | L260 | 16 47 06.7 | −09 35 21 | 16442-0930 | Ophiuchus | 120 | 4 | 1.6 | ··· | <7.9 | 15.8 | 2,*,10,5 |
| 60 | L158 | 16 47 23.2 | −13 59 21 | 16445-1352 | Ophiuchus | 120 | 4 | <2.8 | <1.7 | <7.0 | 4.0 | 4,4,4,5 |
| 61 | L191 | 16 47 29.3 | −12 28 38 | ··· | Ophiuchus | 120 | 4 | <2.8 | <1.7 | <6.4 | 0.71 | 4,4,4,5 |
| 62 | L204F | 16 47 48.4 | −11 56 56 | ··· | Ophiuchus | 120 | 4 | <2.9 | <1.7 | <6.1 | 1.43 | 4,4,4,5 |
| 63 | L234A | 16 48 06.9 | −10 51 48 | 16451-1045 | Ophiuchus | 120 | 4 | <3.3 | ··· | <3.2 | 5.0 | 2,*,10,5 |
| 64 | L234E | 16 48 08.6 | −10 56 58 | 16451-1054 | Ophiuchus | 120 | 4 | 2.1 | ··· | ··· | 2.5 | 2,*,*,5 |
| 65 | L63 | 16 50 15.5 | −18 06 06 | ··· | Ophiuchus | 120 | 4 | 2.3 | 3.9 | <5.1 | 7.9 | 2,1,1,1 |
| 66 | B68 | 17 22 38.8 | −23 50 02 | ··· | other | 200 | 3 | 3.0 | 18.9 | 7.8 | 2.5 | 4,4,4,5 |
| 67 | L492 | 18 15 46.1 | −03 46 13 | ··· | Aquila | 200 | 6 | 53 | 172 | 41 | 3.4 | 12,12,12,12 |
| 68 | L429-1 | 18 17 05.6 | −08 13 30 | ··· | Aquila | 200 | 6 | 14.2 | 7.5 | <6.4 | 10.4 | 4,4,4,4 |

Table A.1—Continued

| No | Source Name | RA(J2000) | Dec(J2000) | YSO(*IRAS*) Name | Region | Distance (pc) | Ref. | $N$[CCS] ($10^{12}$ cm$^{-2}$) | $N$[$HC_3N$] ($10^{12}$ cm$^{-2}$) | $N$[$HC_5N$] ($10^{12}$ cm$^{-2}$) | $N$[$NH_3$] ($10^{14}$ cm$^{-2}$) | Ref. |
|---|---|---|---|---|---|---|---|---|---|---|---|---|
| 69 | L483 | 18 17 29.7 | −04 39 38 | 18148-0440 | Aquila | 200 | 3 | 12.3 | 31 | 17.6 | 14.9 | 4,4,4,4 |
| 70 | L530H | 18 49 28.5 | −04 57 40 | ··· | Aquila | 350 | 3 | <3.8 | <2.0 | <8.4 | <0.65 | 4,4,4,5 |
| 71 | L530D | 18 50 02.7 | −04 49 09 | ··· | Aquila | 350 | 3 | 4.1 | <1.5 | <5.4 | <0.09 | 4,4,4,4 |
| 72 | B133 | 19 06 06.9 | −06 52 41 | ··· | Aquila | 400 | 3 | 7 | ··· | ··· | 2.89 | 2,*,*,5 |
| 73 | L723 | 19 17 53.9 | +19 12 19 | 19156+1906 | other | 300 | 3 | <2.8 | <1.3 | <2.8 | 1.6 | 1,1,1,1 |
| 74 | L778 | 19 26 32.6 | +23 58 42 | 19244+2352 | other | 200 | 3 | 4.5 | 4.3 | 6.1 | 2.8 | 1,1,1,1 |
| 75 | B335 | 19 36 59.0 | +07 33 47 | 19345+0727 | other | 250 | 3 | 2.9 | 4.2 | <2.2 | 1.3 | 2,1,1,1 |
| 76 | L1152 | 20 35 50.3 | +67 54 22 | 20353+6742 | Cepheus | 325 | 3 | <4.2 | ··· | ··· | 7.9 | 2,*,*,5 |
| 77 | L1157 | 20 39 06.6 | +68 02 13 | 20386+6751 | Cepheus | 325 | 3 | <2.3 | 1.64 | ··· | 5.2 | 8,4,*,13 |
| 78 | L1147 | 20 40 31.9 | +67 20 25 | ··· | Cepheus | 325 | 3 | 5.5 | 4.5 | <5.9 | 0.08 | 4,4,4,4 |
| 79 | L1155H | 20 43 06.5 | +67 46 26 | ··· | Cepheus | 325 | 3 | <2.4 | <1.6 | <5.4 | <0.82 | 4,4,4,5 |
| 80 | L1155C | 20 43 30.0 | +67 52 42 | ··· | Cepheus | 325 | 3 | 5.2 | 2.4 | ··· | 5.0 | 8,4,*,5 |
| 81 | L1155D | 20 43 49.8 | +67 36 29 | ··· | Cepheus | 325 | 3 | <2.8 | <1.6 | <5.7 | <0.34 | 4,4,4,5 |
| 82 | L1082A | 20 53 30.2 | +60 14 46 | 20520+6003 | Cepheus | 440 | 3 | 2.6 | 3.3 | <1.7 | 1.5 | 2,2,2,2 |
| 83 | L1082B | 20 53 52.2 | +60 11 18 | 20526+5958 | Cepheus | 440 | 3 | <1.3 | <0.7 | <2.2 | 0.6 | 2,2,2,2 |
| 84 | L1228 | 20 59 30.6 | +78 22 49 | 21004+7811 | Cepheus | 150 | 3 | <2.4 | 2.3 | ··· | 1.74 | 8,4,*,5 |
| 85 | L1172A/L1172D | 21 02 23.2 | +67 54 35 | 21017+6742 | Cepheus | 288 | 3 | 4.9 | 21 | 14.4 | 7.9 | 4,4,4,5 |
| 86 | L1172B(-120,-40) | 21 03 10.6 | +68 11 17 | ··· | Cepheus | 288 | 3 | 4.0 | 4.4 | <5.2 | 0.81 | 4,4,4,4 |
| 87 | L1172B(-40,-40) | 21 03 24.9 | +68 11 18 | ··· | Cepheus | 288 | 3 | 4.6 | 6.4 | <5.0 | <0.13 | 4,4,4,4 |
| 88 | L1172B(+40,+40) | 21 03 39.1 | +68 12 39 | ··· | Cepheus | 288 | 3 | 6.4 | 4.2 | <4.8 | <0.13 | 4,4,4,4 |
| 89 | B361 | 21 12 13.2 | +47 24 24 | 21106+4712 | other | 350 | 3 | <1.9 | <0.7 | <3.6 | 0.7 | 1,1,1,1 |
| 90 | L1251E | 22 39 17.7 | +75 11 29 | 22376+7455 | Cepheus | 300 | 3 | 6 | ··· | ··· | 3.1 | 2,*,*,14 |

Note. — References for distances — 1: Hirota et al. (2008); 2: Torres et al. (2007); 3: Hilton & Lahulla (1995); 4: Loinard et al. (2008); 5: Lee & Myers (1999)

Note. — References for column densities — 1: Suzuki et al. (1992); 2: Benson et al. (1998); 3: Ladd et al. (1994); 4: Present study; 5: Benson & Myers (1989); 6: Hirota et al. (2004); 7: Hirota et al. (2002); 8: Hirota et al. (2001); 9: Ungerechts et al. (1980); 10: Benson & Myers (1983); 11: Mundy et al. (1990); 12: Hirota & Yamamoto (2006); 13: Bachiller et al. (1993); 14: Anglada et al. (1997)